

FLOOR VIBRATION ISOLATION OF A CORIOLIS MASS-FLOW METER USING FILTERING TECHNIQUES

K.L.J. Stroeken

EEMCS/SC
MECHANICAL AUTOMATION AND MECHATRONICS

EXAMINATION COMMITTEE

Dr.ir. R.G.K.M. Aarts

Dr.ir. W.B.J. Hakvoort

Dr.ir. F. van der Heijden

DOCUMENT NUMBER

WA - 1505

CONFIDENTIAL

SAMENVATTING

In dit onderzoek is de onderdrukking van vloertrillingen en andere verstoringen met behulp van filtertechnieken en additionele sensoren onderzocht. Een door Bronkhorst gemaakte Coriolis Massa-Flow Meter (CMFM) voor kleine massa-flow is gebruikt om inzicht te krijgen in de werking van dergelijke filters. Het verbeteren van deze CMFM bestaat uit twee stappen. Allereerst wordt een voorspelling gedaan van de invloed van de verstoringen op de meetfrequentie. Hierna worden de overige verstoringen zo goed als mogelijk weg gefilterd uit het meetsignaal.

In het eerste deel, de voorspelling, zal eerst een overdrachtsfunctie van vloertrillingen naar massa-flow worden bepaald. Met deze overdracht wordt er een model gemaakt op basis van toestandsvergelijkingen. De gemeten vloertrillingen worden dan met behulp van deze vergelijkingen omgezet in een geschatte massa-flow fout. Na het aftrekken van de geschatte fout van het massa-flow meetsignaal is er bij voldoende vloertrilling een verbetering te zien in de gemeten flowwaarde van 20dB.

Het tweede deel van het onderzoek, is gefocust op het zo goed mogelijk verwijderen van ruis en verstoringen die nog aanwezig zijn na de correctie met behulp van voorspelling. Hiervoor wordt het tijdsignaal gefilterd door een notch filter. Om dit filteren mogelijk te maken gaat het signaal eerst door een laagdoorlaatfilter. Hierna wordt het geresampled en gefilterd voordat de flow uitgerekend wordt. De berekende flow wordt dan nog een keer gefilterd waarbij hoogfrequente ruis en verstoringen worden verwijderd. Dit geeft nog eens 6 tot 24dB verbetering ten opzichte van het huidige filteralgoritme, afhankelijk van de gewenste responsietijd.

ABSTRACT

In this research, narrow-band floor vibration isolation using filtering techniques was evaluated. A Bronkhorst Coriolis Mass Flow Meter, CMFM, for low flows is used as a platform for testing the rejection of the effect of external disturbances on the measurement signal. The robustification of this CMFM consists of both predicting the disturbance at the sensing frequency and removing as much of the other disturbances as possible.

The first part, the prediction, starts with estimating the transfer from floor vibrations to mass-flow measurements. Once this transfer is obtained, it is modeled using a state space model. The measured floor vibrations are fed to this model and then subtracted from the measured mass-flow. This technique attenuates the influence of floor vibrations on the measured mass-flow by 20dB.

The second part is the removal of the remaining disturbances (floor vibrations, noise and higher harmonics). This is done using a notch and a Bessel filter. In order to enable notch filtering the signal is low-pass filtered and resampled after which it can be filtered. After flow calculation, a second order Bessel filter removes any high-frequent noise still present in the flow signal. This filtering gives another 6 to 24dB more attenuation than the techniques currently used in the CMFM.

PREFACE

The last project for obtaining a Master of Science degree is an individual project of 40 European Credits. Before I'm going to tell you about what I did in this research, I want to give you a little insight into the way I got here.

I remember being a little scared and excited coming to Enschede as a "feut" to start studying Electrical Engineering. Since I'm from the south of the Netherlands, a hamlet called Nieuw Bergen, I had to look for a room. I was lucky to find one in the best student residence on campus: "CLUB 9-2". After an awesome ten days introduction period of partying and getting to know my fellow students, the first lectures hit me hard; this wasn't high school anymore! Eventually, after some warming up I had no real trouble finishing my Bachelor Degree.

Then what?! Then you get to choose again. This time I had to make a decision on which Master program and courses I was going to follow. I already had some work experience in Mechanical Engineering and decided that was the way to go. In consultation with Ronald Aarts, he and I decided that if I followed the Master Systems and Control with some Mechanical Engineering courses, I could finish this Master at the Mechanical Automation chair. The courses were a lot more interesting than the Bachelor courses and especially the projects were great fun.

After finishing up the courses, it was time to show the people what I had learned over the years. For me, this started by going abroad to participate in an engineering internship in Colombia. A project focused on the modeling and control of two parallel manipulators was a nice challenge, which I finished with good result. After spending a few more weeks on vacation in this amazing country, it was time to get back and start graduating.

I found this assignment, that combines Electrical and Mechanical Engineering, challenging. Picking up on a research that started in 2003 is not easy. Luckily Bert, my daily supervisor, had some really neat preliminary research and after some trial and error, I was able to contribute to the project.

Finally after 7 months of hard work and getting used to the 9 to 5 working hours, this report is laying on my desk. It's too bad that this also means the end to an era of studying and fun (not necessarily in that order), but I feel ready and excited to look for a new challenge.

For you, dear reader, the next challenge will be reading all of the things I've put down here, while I will have some time to catch my breath.

TABLE OF CONTENTS

Samenvatting	I
Abstract.....	II
Preface	III
Table of Contents	IV
1 Introduction.....	1
2 Theory	3
2.1 Coriolis Mass Flow Meters	3
2.2 Disturbances	8
2.3 Transfer Function	10
2.4 Prediction Filters	11
2.5 Band-Pass Filters	14
3 Implementation and Results.....	17
3.1 Experimental Setup.....	18
3.2 Gain Estimation	20
3.3 Prediction Filter	21
3.4 Notch Filter.....	24
4 Conclusion.....	28
5 Discussion.....	29
References.....	30
Appendix A: Phase Locked Loop.....	31
Appendix B: Online Gain Estimation and DQDM Filtering.....	35

1 INTRODUCTION

For continuous production and batch processes, for instance in the pharmaceutical industry, it is sometimes necessary to measure small mass quantities of liquids and gasses. To correctly measure such small mass-flows, a sensor is being developed by Bronkhorst High-Tech based on the Coriolis principle. This type of sensor is able to directly measure mass quantity passing through a tube. Currently there are Coriolis devices commercially available that measure flows as small as 1g/h (1).

However, there is a problem with the further scaling down of these devices. External vibrations from pumps or other equipment generate measurement errors. The cause for this is the fact that the measured Coriolis force, induced by a mass-flow, cannot be distinguished from forces caused by vibrations. Measurement errors increase as the Coriolis force decreases more from scaling down than vibration forces.

Currently, there is research being done to make Coriolis Mass Flow Meters, or CMFMs, less vulnerable to external vibrations. There are projects that focus on passive and active vibration isolation removing disturbances from the tube (2). These solutions however, are costly and can add asymmetry to the device resulting in an incorrect flow measurement.

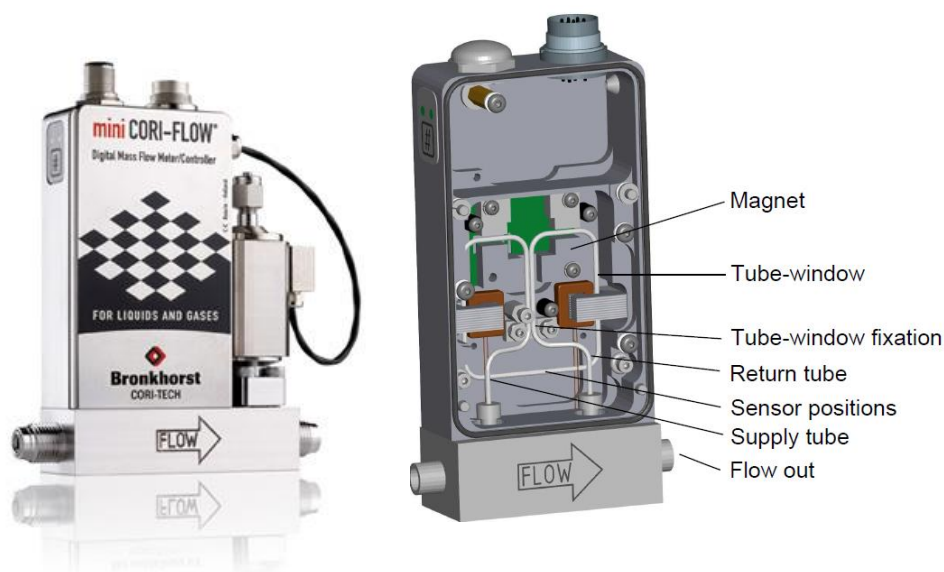


FIGURE 1 - BRONKHORST CORIOLIS MASS FLOW METER (LEFT) AND DETAILED SKETCH (RIGHT)

In this research, the CMFM in figure 1 is robustified by measuring the external vibrations, predicting their effect on the flow measurement and correct for it. Therefore, no extra stages are added to the measurement device.

An extra sensor is placed on the case to measure external disturbances. Models and filtering algorithms improve the accuracy of the measured mass-flow using these extra measurements. This prediction algorithm should add 20dB disturbance attenuation while achieving a response time of less than one second. Furthermore, the options of removing disturbances by band-pass filtering the time-domain signal are also investigated.

The next chapter expounds the workings of a CMFM before going into detail on the disturbances affecting this type of sensor. In paragraph 2.4, the theory behind the prediction filter is expounded. This filter requires a transfer estimate from external vibrations to a measurement error which is obtained in paragraph 2.3. The last part of chapter 2 is focused on band-pass filters after which both filters are implemented and tested in chapter 3. The last two chapters of this thesis review the work in the form of conclusions and a discussion of the used approach.

In the appendices some extra information can be found on less successful algorithms. The first appendix deals with the Phase Locked Loop. This is used for estimating signal parameters of the actuation signal and an attempts was made to measure flow by means of this PLL. Also, in order to implement the prediction filter, an attempt was made to enable online gain estimation by extra filtering and a Recursive least squares algorithm. This is explained in appendix b.

2 THEORY

In this chapter some theoretical background of the sensor workings is explained before taking a closer look at the disturbances acting on the sensor. These paragraphs are mainly based on prior research (1), (3) and (4). In the third paragraph the first added work is seen in the form of deriving the transfer function from the disturbances to the measurement error after which this information is used for the prediction filter in paragraph 2.4. The last part of this chapter explains the contribution and workings of a band-pass filter.

2.1 CORIOLIS MASS FLOW METERS

Before going more into detail on the research, the workings of a Coriolis Mass Flow Meter are explained. The measurement principle of CMFMs is based on the acceleration and deceleration of a moving mass in a rotating frame. For the sake of explaining this principle, the motion of three particles through a rotating tube is examined. A top view of the tube is depicted in figure 2.

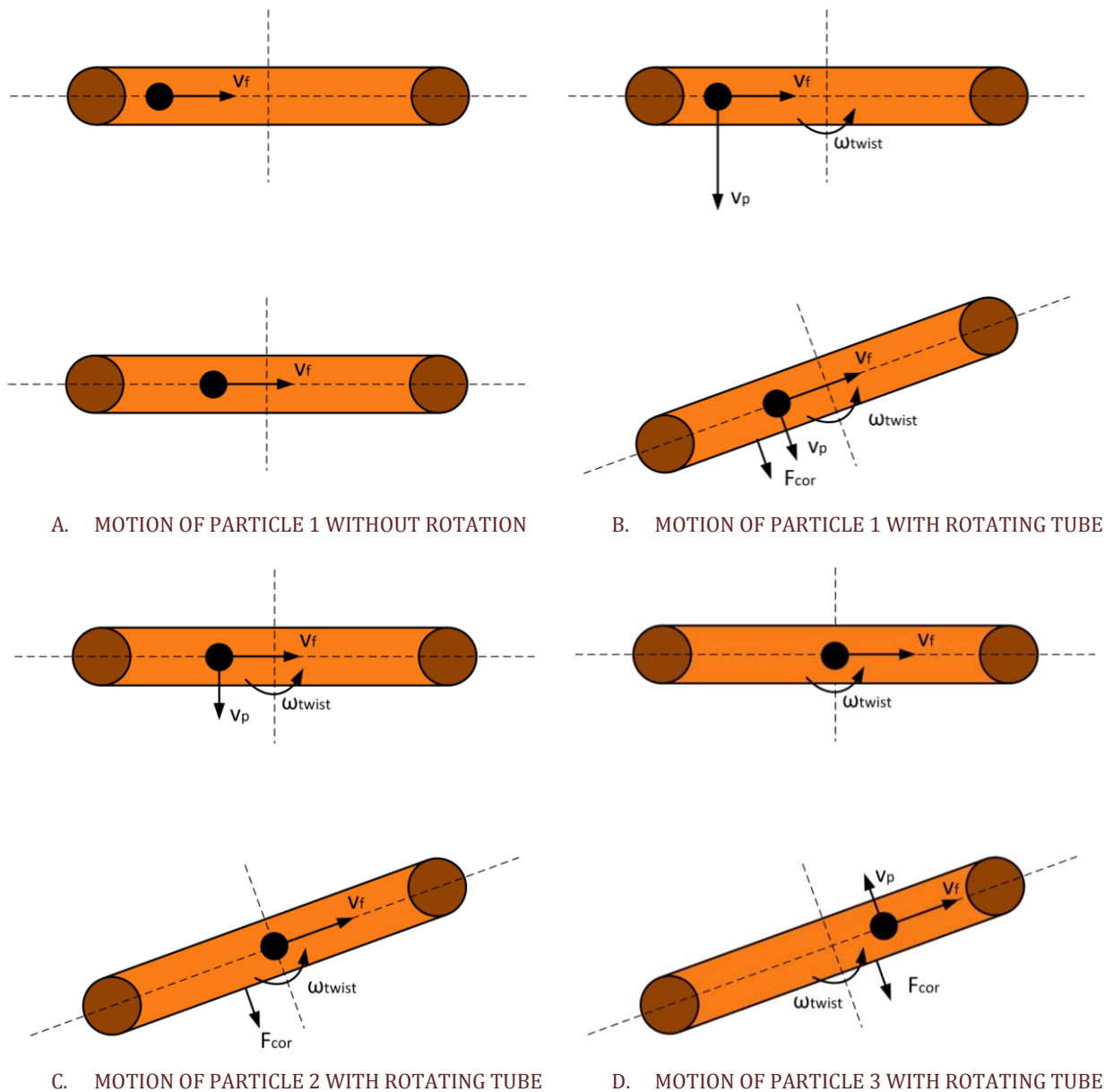


FIGURE 2 - MOVING PARTICLES THROUGH A TUBE

In figure 2a, a mass-flow from left to right is depicted by a particle moving through a tube with a constant flow velocity v_f . The upper tube of figure 2a displays the position of the particle at $t=0$. At the next time instance, displayed in the lower half of figure 2a, the particle moved towards the right representing mass-flow. Next, the tube is rotated around its center with a constant angular velocity ω_{twist} . Again the upper pictures show the state at $t=0$ and the lower pictures show $t=1$; the next time instance.

For particle 1 this is seen in figure 2b. The upper figure shows that due to the angular velocity of the tube, ω_{twist} , particle 1 has a velocity v_p at $t=0$. At the next time instance, $t=1$, the tube rotated and the particle moved towards the axis of rotation due to its flow velocity v_f . As the angular velocity remained constant and the particle moved towards the axis of rotation the velocity v_p decreased. By Newton's law $F = m \cdot a$ this deceleration caused a force on the tube called the Coriolis force and depicted by F_{cor} .

The same can be seen for particle 2 in figure 2c. This particle also moves towards the center of the tube. Just like particle 1 the particle velocity v_p due to the angular velocity decreases during this movement. This causes a similar Coriolis force on the tube, as the deceleration is equal.

In figure 2d, a third particle is now moving away from the axis of rotation. As it moves away, the particle velocity v_p now increases due to the constant angular velocity ω_{twist} and an increased distance from the center of rotation. This also causes a reaction force F_{cor} on the tube in the opposite direction of the acceleration. It should be noted that the direction of the accelerating particle causes a force in the same direction as the force of the decelerating particles. Summing over all particles, the rotating tube experiences a Coriolis force F_{cor} proportional to the mass-flow v_f .

The magnitude of the Coriolis force is calculated using the acceleration and mass of each moving particle and summing over all particles in the tube. Each particle velocity v_p is given by

$$v_p = \omega_{twist} \times x_f \quad (2.1)$$

where x_f is the position of the particle relative to the center of rotation. The particle acceleration can be written as the derivative of (2.1)

$$a_p = 2 \cdot (\omega_{twist} \times v_f) \quad (2.2)$$

Next, the Coriolis force acting on the tube is calculated using the particle mass m_p . Note that this force has an opposite direction than the force acting on the accelerating particle.

$$F_{cor} = -2 \cdot m_p \cdot (\omega_{twist} \times v_f) \quad (2.3)$$

Now, instead of looking at one particle, there is a continuous flow consisting of infinite small particles. The tube has a length, L , and sectional area, A . Here, dl is used as the integration variable over the tube length and represents the infinite small length of a cross-section of the tube. The Coriolis force for each length dl is given by

$$F_{cor} = -2 \cdot (\omega_{twist} \times v_f) \cdot \rho A dl \quad (2.4)$$

where ρ is the mass-density of the flow.

Integrating over the length of the tube gives

$$F_{cor} = \int_{l=-\frac{1}{2}L}^{\frac{1}{2}L} -2 \cdot (\omega_{twist} \times v_f) \rho A dl = -2L\omega_{twist} \times v_f \rho A \quad (2.5)$$

Now, instead of a continuously rotating tube, it is much easier to construct an oscillating tube. The principle of the Coriolis effect still holds. This effect generates a force on the tube proportional to the length of the rotating tube, the mass-flow and the angular velocity. From (2.5) and recognizing $v_f \rho A$ as the mass-flow, \dot{m} , the Coriolis force on the tube can be written as

$$F_{cor} = -2L(\omega_{twist} \times \dot{m}) \quad (2.6)$$

This Coriolis force arises at a tube section normal to the rotation axis. Simultaneously, its direction is perpendicular to the tube window as can be seen in figure 3. Here the tube section examined in figure 2 is the lower part of the tube window.

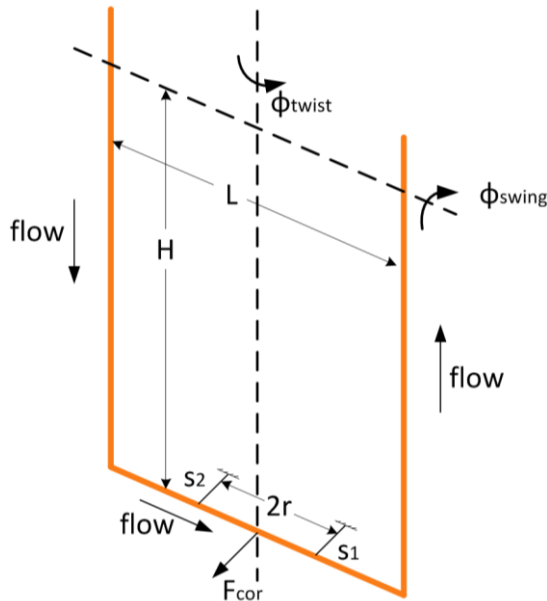


FIGURE 3 - THE TUBE WINDOW

The generated Coriolis force causes tube motion around the swing axis of the tube window with the same frequency as the actuated twist motion. The swing motion caused by the Coriolis force is 90 degrees out of phase with the actuation. This is because a force proportional to the velocity of the actuation motion actuates it. Two sensors are placed on opposite sides of the actuation axis measuring both actuation (twist) and swing (Coriolis) motion. For small motions the sensor signals are almost equal to

$$\begin{aligned} s_1 &\cong -r \cdot \phi_{twist} + h \cdot \phi_{swing} \\ s_2 &\cong r \cdot \phi_{twist} + h \cdot \phi_{swing} \end{aligned} \quad (2.7)$$

with the actuated motion given by

$$\phi_{twist} = a \cdot \sin(\omega_{act} \cdot t) \quad (2.8)$$

where ω_{act} is the actuation frequency. According to (2.6) the actuated motion will cause a Coriolis swing motion proportional to the mass flow

$$\phi_{swing} = b \cdot \dot{m} \cdot \cos(\omega_{act} \cdot t) \quad (2.9)$$

Using (2.7), (2.8), (2.9) and some trigonometry the time-varying sensor signals can be written as

$$\begin{aligned} s_1 &= c \cdot \sin(\omega_{act} \cdot t + \theta_1) \\ s_2 &= c \cdot \sin(\omega_{act} \cdot t + \theta_2) \end{aligned} \quad (2.10)$$

where $\theta_1 - \theta_2 = \pi$ if no mass is flowing through the tube and thus no Coriolis motion is generated. This is due to the sensors being at opposite sides of the twist axis.

The contribution of (2.9) to (2.10) gives an extra, opposite phase shift between s_1 and s_2 in θ_1 and θ_2 . This phase shift is a direct measure of the amount of mass flowing through the tube. Multiplied with a sensor sensitivity, S , there is a linear approximation between the mass-flow and the phase difference θ which holds for small phase angles

$$\dot{m} \cong S \cdot \frac{2b}{a} = S \cdot \theta = S \cdot (\theta_1 - \theta_2 - \pi) \quad (2.11)$$

where the sensor sensitivity is based on material properties and tube window dimensions.

A Dual Quadrature Demodulation scheme (DQDM) (3) is used to measure the phase difference between the two sensor signals.

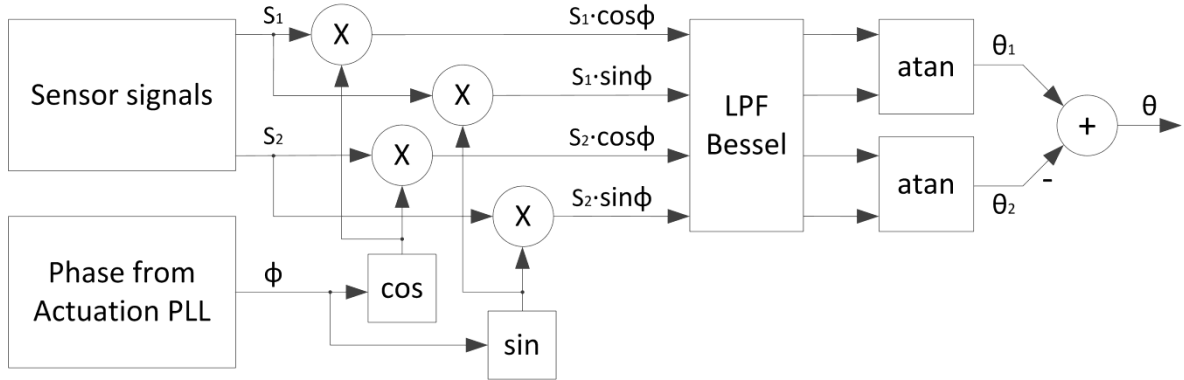


FIGURE 4 - DUAL QUADRATURE DEMODULATION SCHEME

From figure 4, the equations corresponding to the DQDM phase calculation are derived. First, both sensor signals are multiplied with the cosine and sine of the actuation (twist) signal. The latter two signals are obtained from a phase locked loop (PLL) used for estimating the actuation frequency and phase. This signal multiplication is called mixing and converts the signal frequency.

Mixing generates two signals; one with the original frequency subtracted from the mixing frequency and one where the signal frequency is added to the mixing frequency

$$\cos(\omega_1 t) \cdot \cos(\omega_{mix} t) = \frac{1}{2} \cos((\omega_{mix} - \omega_1) t) + \frac{1}{2} \cos((\omega_{mix} + \omega_1) t) \quad (2.12)$$

In this case mixing is done with the signal frequency, resulting in a DC component of the signal and the second harmonic of the signal frequency.

For the first sensor signal the result after mixing is written as

$$s_1 \cdot \cos(\phi) = c \cdot \sin(\omega_{act} t + \theta_1) \cdot \cos(\omega_{act} t) = \frac{c}{2} (\sin(\theta_1) + \sin(2 \cdot \omega_{act} t + \theta_1)) \quad (2.13)$$

$$s_1 \cdot \sin(\phi) = c \cdot \sin(\omega_{act} t + \theta_1) \cdot \sin(\omega_{act} t) = \frac{c}{2} (\cos(\theta_1) + \cos(2 \cdot \omega_{act} t + \theta_1)) \quad (2.14)$$

Applying a low pass filter (LPF) to the mixed signals removes the second harmonic. A Bessel filter is used as it has a constant delay for all pass-band frequencies. This means that no matter the change rate of the flow there is a constant delay in the filter. Therefore, the total flow is most correctly calculated.

Low-pass filtering (2.13) and (2.14) gives

$$\frac{c}{2} (\sin(\theta_1) + \sin(2 \cdot \omega_{act} t + \theta_1)) \xrightarrow{LPF} \frac{c}{2} \sin(\theta_1) \quad (2.15)$$

$$\frac{c}{2} (\cos(\theta_1) + \cos(2 \cdot \omega_{act} t + \theta_1)) \xrightarrow{LPF} \frac{c}{2} \cos(\theta_1) \quad (2.16)$$

the arctangent of the filtered signals gives the phase of the sensor signal

$$\arctan\left(\frac{\frac{c}{2} \cos(\theta_1)}{\frac{c}{2} \sin(\theta_1)}\right) = \theta_1 \quad (2.17)$$

where the calculated phase does not depend on the signal amplitude c .

The same path is followed for the second sensor signal giving the phase θ_2 . From (2.11) and the measurement sensitivity, the mass-flow is calculated. This calculated mass-flow can be disturbed by external vibrations causing measurement errors. In the next paragraph, more information on such disturbances is given.

2.2 DISTURBANCES

In this paragraph, the effect of external vibrations on the measurement error of Coriolis mass-flow meters is explained. To this end the disturbance directions are identified and their effect on the measurement is evaluated. Also, the sensor placement for measuring the correct disturbances is discussed.

In a prior research done by Van de Ridder (4), the major disturbance directions of CMFMs were identified. In that research a model of the sensor window was constructed using the multi-body modeling tool SPACAR (5). In figure 5, the first four eigenmodes of this model are depicted and their natural frequencies are given. It should be noted that the Coriolis force causes a swing motion at the frequency of the actuation (twist) mode and although it causes similar motion it does not excite the first swing mode in its eigenfrequency. The frequencies in figure 5 can change by a maximum of plus or minus five percent due to flow density and temperature differences. The filtering algorithms should be able to cope with these varying frequencies.

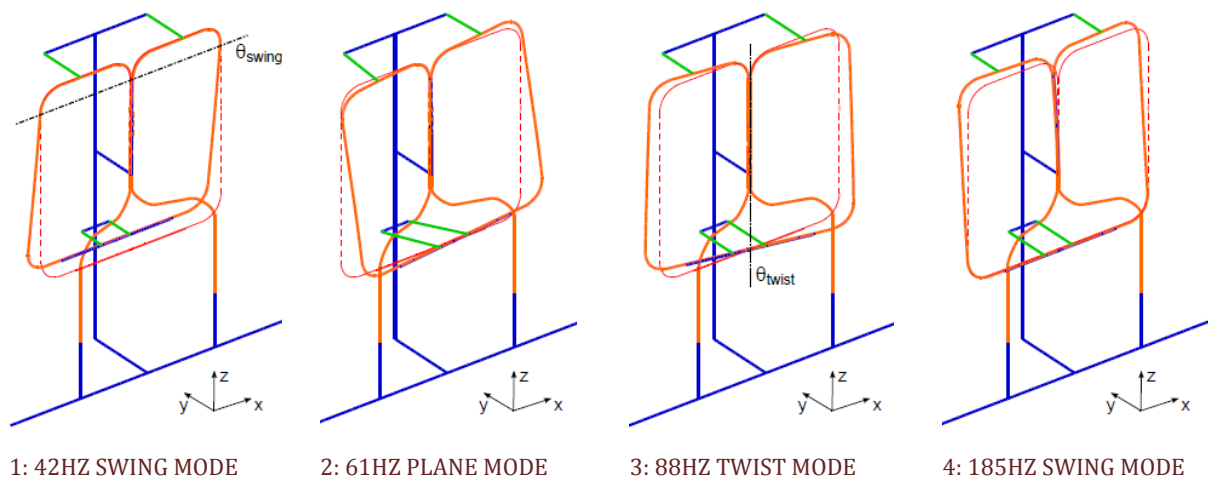


FIGURE 5 - THE FIRST FOUR MODESHAPES AND CORRESPONDING EIGENFREQUENCIES OF THE WINDOW

A multi-sine (1-550Hz) in all six degrees of freedom has been presented to the casing while the flow, was measured. By using the floor accelerations and flow measurements, a transfer was estimated from each disturbance to the measurement value. It showed that a disturbance in the y-direction had 50dB more contribution to the measurement error than any other disturbance. This is understood when noticing that the displacement caused by the Coriolis force is the same as the first swing mode. It is easy to see that the first swing mode is excited by a rotation around the x-axis or a y-displacement. Experiments show that y-displacements have a much larger contribution than x-rotations.

In order to measure the disturbances, a sensor is needed. This sensor should only measure disturbances that cause measurement errors. Therefore, these disturbances should not be measured on the tube window as it is not known whether the measured motion is caused by the Coriolis force or external disturbances. The transfer from the case to the tube displacement can be determined. This means that the best location for a disturbance sensor is on the case.

As stated, the sensor should be able to measure y-disturbances. The position where these disturbances play the biggest role is in the tube window's center of moving mass for the first swing mode. This location is at a z-position 5% of the height h of the tube window depicted in figure 6. At this position, disturbance rotations about the x-axis that contribute to the measurement error are also measured as y-displacements, making it the ideal position. By placing the sensor in this point maximum attenuation can be achieved with only one sensor.

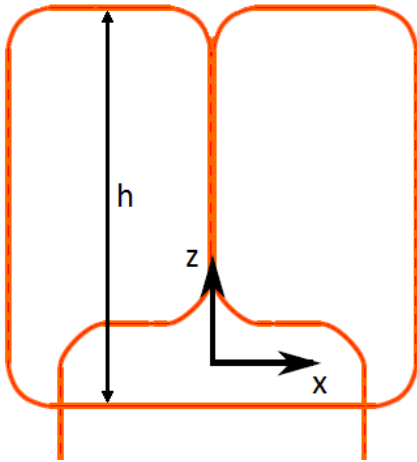


FIGURE 6 - SENSOR PLACEMENT

The x-position of the sensor has to be on the twist axis i.e. the center of the tube window. This ensures that no actuation motion is measured.

The sensor-type is an acceleration sensor as this is the most convenient device for measuring disturbances.

The next section will focus on the transfer from the disturbances, identified in this paragraph, to the measured flow.

2.3 TRANSFER FUNCTION

In this paragraph, the transfer from disturbances perpendicular to the tube window, a_y , to Coriolis displacement Δx is derived. In figure 7, a simplified disturbance model is shown. Despite its simplicity it is a good model of the system, as only one disturbance direction and mode are dominant in the effect of external vibrations on the flow measurement.

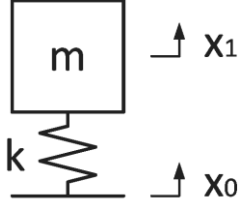


FIGURE 7 - SIMPLIFIED MODEL FOR DERIVING THE TRANSFER FROM VIBRATIONS TO CORIOLIS DISPLACEMENT

From this model the transfer function is derived

$$\Delta x = x_1 - x_0 \quad (2.18)$$

$$x_1 = \frac{1}{m \cdot s^2} \cdot F \quad (2.19)$$

$$x_0 = \frac{a_y}{s^2} \quad (2.20)$$

$$F = \Delta x \cdot k \quad (2.21)$$

$$\omega_{swing} = \sqrt{\frac{k}{m}} \quad (2.22)$$

$$\Delta x = \frac{1}{m \cdot s^2} \cdot \Delta x \cdot k - \frac{a_y}{s^2} \quad (2.23)$$

$$\Delta x \cdot s^2 = -\frac{k}{m} \cdot \Delta x - a_y \quad (2.24)$$

$$\Delta x \cdot (s^2 + \omega_{swing}^2) = -a_y \quad (2.25)$$

$$\frac{\Delta x}{a_y} = -\frac{1}{s^2 + \omega_{swing}^2} \quad (2.26)$$

Conversion of a_y and Δx to volts in the setup, gives rise to a scaling factor g . The total transfer from floor accelerations to Coriolis displacement is then given by

$$\frac{V_{out}}{V_{in}} = \frac{g}{s^2 + \omega_{swing}^2} \quad (2.27)$$

The gain parameter, g , scales the transfer function and needs to be estimated accurately. This is done by identifying the transfer function from disturbance input to swing motion in paragraph 3.2. Note that the gains can be different for sensor 1 and sensor 2.

2.4 PREDICTION FILTERS

With the transfer from paragraph 2.3, a prediction filter is built that estimates the influence of the disturbances and directly subtracts them from the measurements. Recall from section 2.2, that disturbances are only important at the actuation frequency. This is the frequency at which the Coriolis displacement is measured and therefore no information should be removed by band-pass filtering. A prediction filter can in this case present a solution as it does not blindly filter the signal, but makes a prediction of the disturbance's influence. This prediction can then be subtracted from the measured sensor signal to enhance the system output.

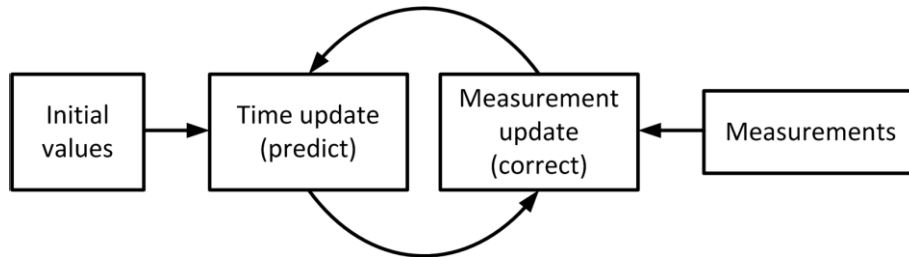


FIGURE 8 - GENERAL PREDICTION FILTER

Prediction filtering is a two-step recursive process as seen in figure 8. First, a prediction is executed based on model information, i.e. the transfer function, the current description of the system; the system's state vector and the input accelerations. During this prediction a state uncertainty matrix is updated. This uncertainty matrix describes the correctness of the state vector. In this case, the new state vector's uncertainty is updated with the model uncertainty. This increases the uncertainty of the state vector, as the model is almost never 100% correct. The second step of prediction filtering is a correction. This update happens when a new measurement is available. During correction the measurement and the prediction are compared and the difference between them is used to calculate the innovation. The innovation describes the amount by which the new system state is corrected. This innovation is based on the measured difference between the state vector and the measurement with both the measurement and the state uncertainty taken into account. If the measurement uncertainty is much greater than the current system state uncertainty, only a small amount of the measured difference is added to the system state vector. If the measurement is more certain than the state, a large amount of this difference is added. This process continuously estimates the best possible system state vector and suppresses the influence of noise. After correction a new state uncertainty is calculated. The state uncertainty after a measurement update always decreases as the measurement adds information. After correction a new prediction is done.

In this research a Kalman prediction filter (6) is used. Other options like particle filters, extended Kalman filters and Infinite Impulse Response Least Mean Squares filters (7) require a lot of computational power or extra noise shaping filters. This makes them more complex and heavier on resources than the relatively simple Kalman filter.

Kalman filters require the system transfer function to be written in state space form

$$x(t + 1) = F(t) \cdot x(t) + L(t) \cdot u(t) \quad (2.28)$$

with

$$x(t) = \text{current state vector}, \quad u(t) = \text{input vector}$$

The transfer function (2.27) is used to obtain the system transition matrix F and input matrix L . The state space transfer function is discretized and the input and transition matrix are calculated. The state space transfer is found to be

$$\begin{bmatrix} \hat{x}_1(n + 1) \\ \hat{x}_2(n + 1) \end{bmatrix} = \begin{bmatrix} 1 & T_s \\ \omega_{swing}(n)^2 \cdot T_s & 1 \end{bmatrix} \cdot \begin{bmatrix} x_1(n) \\ x_2(n) \end{bmatrix} + \begin{bmatrix} 0 \\ T_s \end{bmatrix} \cdot a_y(n) \quad (2.29)$$

where

$$x_2 = \dot{x}_1, \quad g(n) = \text{gain}, \quad T_s = \text{Sample time}, \quad a_y = \text{external disturbance} = V_{in} \cdot g$$

The Kalman filter uses equation (2.29) for predicting the next state. A so-called covariance matrix is used to keep track of the uncertainty. The state covariance matrix for the next state $\hat{C}_x(n + 1)$ is calculated using the process covariance matrix C_w . C_x resembles the state uncertainty whereas C_w gives the uncertainty of the model and input signal. The next state covariance matrix is calculated according to

$$\hat{C}_x(n + 1) = F(n) \cdot C_x(n) \cdot F^T(n) + C_w \quad (2.30)$$

When a new measurement is available, the current state information is updated with this information. Using the measurement noise covariance matrix C_v , the innovation matrix S is calculated

$$S(n) = H \cdot \hat{C}_x(n) \cdot H^T + C_v \quad (2.31)$$

where H is the measurement matrix. In this model the position is measured and therefore the measurement matrix is given by

$$H = [1 \quad 0] \quad (2.32)$$

Using the innovation matrix the Kalman gain matrix is determined

$$K(n) = \hat{C}_x(n) \cdot H^T \cdot S(n)^{-1} \quad (2.33)$$

which allows updating the system state vector and covariance matrix using $y(n)$; the measurement of the CMFM's tube position sensor

$$x(n) = \hat{x}(n) + K(n) \cdot y(n) \quad (2.34)$$

$$C_x(n) = \hat{C}_x(n) - K(n) \cdot S(n) \cdot K(n)^T \quad (2.35)$$

After obtaining an updated state a new prediction is done according to (2.29) and (2.30).

The covariance matrices should be initially set to large uncertainties as the start-up state of the system is unknown. This results in large innovations at start-up where the filter relies a lot on its measurements. After some time, the system state becomes more certain and the innovations will decrease. The filter relies more on the transition matrix to obtain its next state. Finally, the Kalman gain matrix will become a steady matrix. This is because of the constant measurement and input covariance gives a constant certainty ratio of measurement and predicted state.

Although being constant, the innovation, Kalman gain and covariance matrices are continuously updated. This consumes a lot of processing power just to have faster convergence at start-up. Since the Coriolis Mass Flow Meters are generally used during long-term operation, this recalculation is unnecessary. Therefore a steady state Kalman gain matrix is calculated using the process, measurement and input covariance matrices and MATLAB's `dlqe` command. This reduces the number of equations for one correct and predict cycle, from six to two: (2.29) and (2.34).

The prediction filter is able to predict the influence of disturbances at the actuation frequency. Around this frequency leftover disturbances and noise should be filtered away to obtain a better signal to noise ratio (SNR). In the next paragraph, the contribution of such band-pass filters is discussed.

2.5 BAND-PASS FILTERS

Filtering the signal before and during processing can massively improve the signal to noise ratio, SNR, of the final measurement. As explained in paragraph 2.1, the dual quadrature demodulation scheme has a low-pass filter after the mixer to remove noise from the measurement. The bandwidth of this filter is in direct correlation with the sensor's response time, e.g. if a 10Hz wide low pass filter is used, the fastest response time is 0.1s. If this low pass filter is projected at the actuation frequency using (2.12) a 10Hz low-pass filter effectively becomes a 20Hz band-pass filter.

In theory, a wide filter is required to achieve a decent response time after phase calculation. However, the bandwidth of the same response in the time signal is much smaller. This can be seen when looking at the frequency change due to a changing mass-flow. From (2.11) it follows that a mass-flow causes a phase difference. When the mass-flow, and thus the phase changes, a temporary frequency shift is measured in the time signal. For one of the two sensor signals the phase change, and thus the frequency shift, is positive, while for the other it is negative. The shift is equally divided between the two sensor signals. To measure the temporary frequency shifts a bandwidth around the signal frequency is needed. The required bandwidth in the time domain is calculated from the maximum flow change, $\Delta flow_{max}$, the desired response time, t_r , and the sensor sensitivity, S ,

$$BW_{filt}(Hz) = \frac{\Delta flow_{max}}{2\pi \cdot S \cdot t_r} \quad (2.36)$$

With a measurement sensitivity (2) of $1348 \left(\frac{g}{h \cdot rad} \right)$, a response time of 0.1s and a maximum flow change from -100 to $100 \frac{g}{h}$ the necessary bandwidth can be calculated

$$BW_{filt} = \frac{200}{2\pi \cdot 1348 \cdot 0.1} = 0.24Hz \quad (2.37)$$

Compared to the low-pass filter in the DQDM, the bandwidth needed in the time domain for obtaining the same response is roughly 80 times smaller. If such a filter can be constructed the disturbance rejection is theoretically improved with that same factor, i.e., 38dB.

In practice, band-pass filters for discrete time applications are categorized as either finite impulse response filters, FIR filters, or infinite impulse response filters, IIR filters. FIR filters use only a finite amount of input samples, but are in general more complex than IIR filters. The latter calculate the output value also based on previous output values. This requires less filter coefficients, but results in a filter with infinite memory.

Whilst being slower due to their infinite memory, IIR filters are the best option for this application. From paragraph 2.2 it is recalled that the actuation frequency can change. To obtain correct filter operation, the coefficients need to adapt to this changing actuation frequency. The limited number of coefficients in an IIR filter allows for easier calculation of new, adapted coefficients. Simple FIR filters, like a comb filter, do not have the required small bandwidth required for this time domain filtering. FIR filters with a bandwidth of 2Hz already have 6000 coefficients for 20dB attenuation. Frequency adaptive FIR filters are therefore very difficult to construct.

A notch filter is a simple IIR filter and is used to examine the contribution of band pass filters. The notch filter cancels a specific notch frequency and is almost constant at all other frequencies. The transfer function of a second order notch filter (8) is given by

$$H(z) = \frac{1 + 2\alpha z^{-1} + z^{-2}}{1 + 2\alpha\rho z^{-1} + \rho^2 z^{-2}} \quad (2.38)$$

where the parameter α is based on the normalized notch frequency, ω_0 , as

$$\alpha = -\cos(\omega_0) \quad (2.39)$$

and the normalized bandwidth of the filter is determined by ρ and given by

$$BW = 2 \cdot \arccos\left(\frac{2 \cdot \rho}{1 + \rho^2}\right) \quad (2.40)$$

with $0 < \rho < 1$. The higher ρ gets, the more selective this filter becomes.

Based on equation (2.38), the notch filter equations can be written as two recursive update equations (9) that can be calculated when a new measurement enters the system. The intermediate variable $v(n)$ is used as the memory variable working on both in- and output values. The update equations are given by

$$v(n) = y(n) - \alpha(1 + \rho) \cdot v(n-1) - \rho \cdot v(n-2) \quad (2.41)$$

$$x(n) = v(n) + 2\alpha \cdot v(n-1) + v(n-2) \quad (2.42)$$

and the estimated signal is

$$\hat{c}(n) = y(n) - x(n) \quad (2.43)$$

which represents just the actuation frequency content of the measurement signal $y(n)$ effectively making it a band-pass filter.

The notch frequency of the filter has to be within the range [0.05 ... 0.95] of the Nyquist frequency to guarantee correct filter operation. With the system sample frequency of 24kHz and notch frequency of 88Hz, the signal is resampled 32 times before processing. For a good resampling result, a low-pass anti-aliasing filter is added to the system. This filter removes signal content above the new Nyquist frequency of 375Hz.

By creating multiple resampled datasets, an easy reconstruction of the signal is possible after applying the notch filter. This can best be seen if the resampling is executed during notch filtering. The update equations (2.41) and (2.42) then become

$$v(n) = LPF(y(n)) - \alpha(1 + \rho) \cdot v(n - 32) - \rho \cdot v(n - 64) \quad (2.44)$$

$$x(n) = v(n) + 2\alpha \cdot v(n - 32) + v(n - 64) \quad (2.45)$$

representing the resampled signal with the actuation frequency content removed. Equation (2.43) can again be used to obtain the signal at the actuation frequency.

In the next chapter, this notch filter and the Kalman filter from paragraph 2.4 are combined in order to construct a working filtering algorithm. This algorithm attenuates the influence of floor vibrations on the mass-flow measurement.

3 IMPLEMENTATION AND RESULTS

In this chapter the theory in the previous chapter is combined into one solution. The filtering algorithms are implemented using MATLAB on a Windows personal computer with a 2,8GHz Intel i7 processor and 4GB internal memory. Datasets with measured disturbances are used to check the workings of the proposed algorithms. During these experiments there is no flow and thus the result of the measurement should be 0. Also, step responses are simulated to check the response time of the proposed algorithms. The gains for the prediction filter are estimated in paragraph 3.2. The flow is calculated using the Dual Quadrature Demodulation scheme explained in paragraph 2.1. This is done for a signal without extra filters and a signal with added prediction and band-pass filtering. The influence of both added filtering techniques is evaluated. The complete signal flow chart of processing the measurements is shown in figure 9.

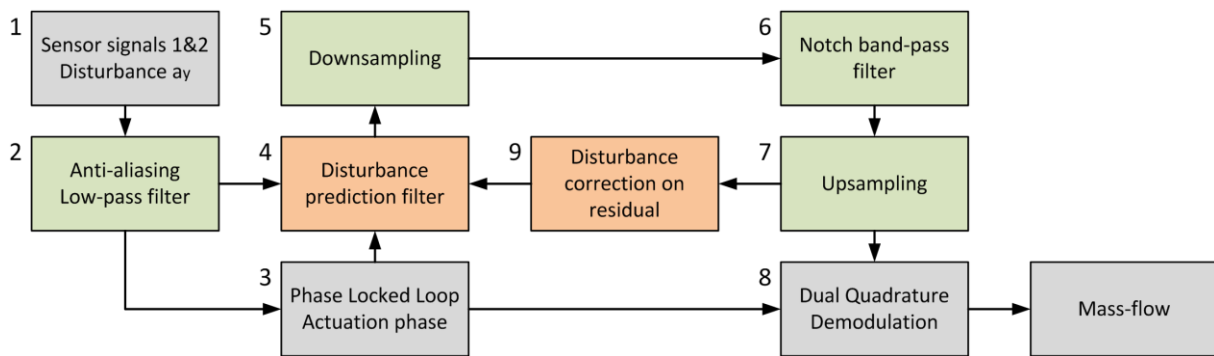


FIGURE 9 - SIGNAL PROCESSING OVERVIEW

The total signal processing algorithm now has nine steps. First, the sensor signals and the disturbance accelerations are measured using opto-sensors and an accelerometer respectively. Next, the measured signals are low-pass filtered. This ensures there is no aliasing when resampling the signal. Thirdly, the actuation frequency and phase are determined using a Phase Locked Loop (10). The workings of such a PLL are expounded in Appendix A. The fourth step is making a prediction of the disturbance based on the measured accelerations and the estimated transfer. After that, the signal is sampled down to enable correct operation of the notch filter. Here, 32 datasets are created such that the signal can be easily reconstructed without information loss. The sixth step is applying the notch filter on the time signal in an attempt to remove disturbances that are not at the actuation/Coriolis frequency. After that, the 32 signals are stitched back together. Step eight is calculating the flow using the Dual Quadrature Demodulation technique, itself consisting of mixing, filtering and phase calculation. The ninth and last step is correcting the disturbance prediction based on the residual. This is the signal with only disturbances and no actuation content.

In the next paragraph, the experimental setup is elaborated after which the gains from disturbances to swing motion are derived using data from this setup. In paragraph 3.3, a prediction filter is constructed using the estimated gains and the workings of this filter are discussed. The last part of this chapter focusses on band-pass filtering and combining all algorithms into one solution.

3.1 EXPERIMENTAL SETUP

For testing purposes, the CMFM is placed on a shaker platform with six degrees of freedom (DOF) (11). This Stewart type suspended platform is actuated by voice coil motors. Co-located acceleration sensors (Endevco7703A-1000) measure the applied disturbances. These disturbances are transformed from the acceleration sensor locations to the Cartesian coordinates depicted in figure 10 using a rigid body model. The setup is shown in figure 10.

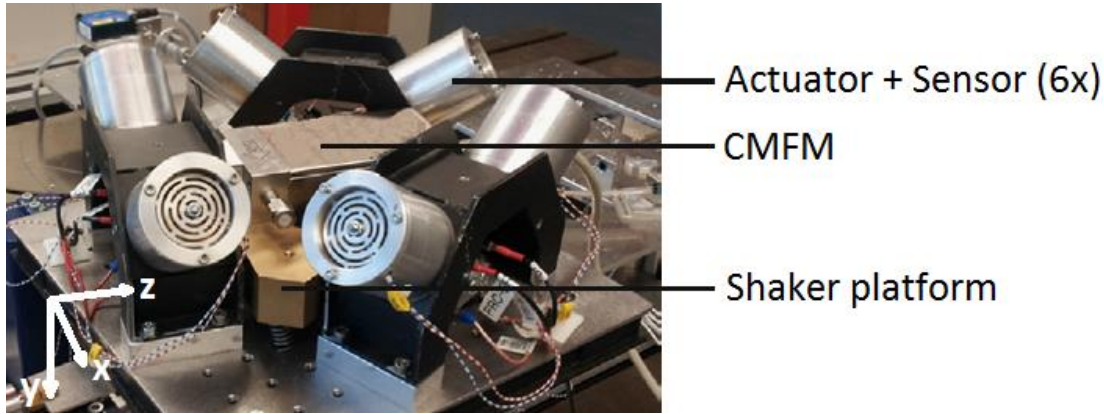


FIGURE 10 - EXPERIMENTAL SETUP: THE CMFM ON THE SHAKER

The disturbance forces are measured using the accelerometers. The response of the CMFM to the disturbances is measured using the opto-sensors also used for measuring mass-flow. Both the accelerometers and the opto-sensors use a National Instruments NI4472 data capturing device able to measure 8 channels with a 24-bit resolution at a sample rate of 24kHz. 60 seconds of data is captured during each experiment. Experiments are executed with and without the CMFM flow-measurement enabled and for varying disturbance levels.

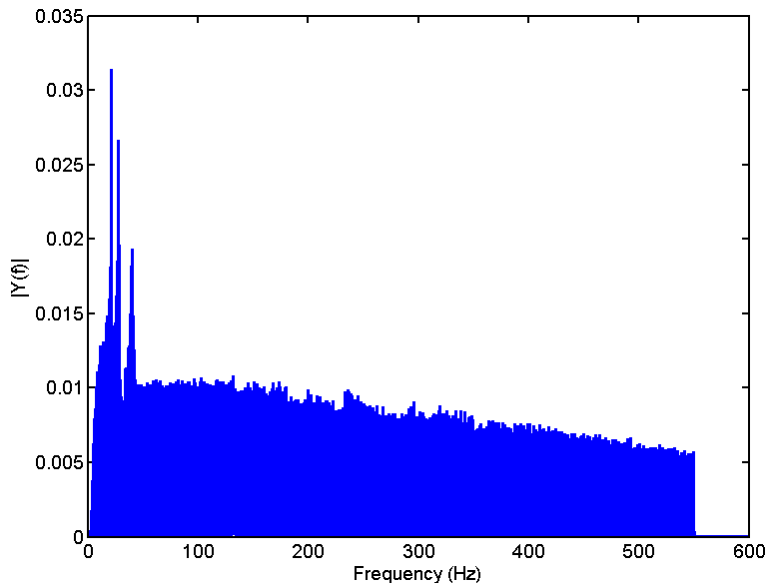


FIGURE 11 - APPLIED DISTURBANCE SPECTRUM

A multi-sine from 1-550Hz is applied to each voice coil motor. The applied disturbance acceleration spectrum can be seen in figure 11. The peaks in this measured disturbance spectrum are the natural frequencies of the shaker. It is possible to compensate for these peaks but as they are not at the actuation frequency this is unnecessary.

In order to gain a little more insight, the signal frequency spectrum of the opto-sensors is depicted in figure 12. Here, the CMFM is turned on, i.e. the twist mode is actuated, enabling flow measurements.

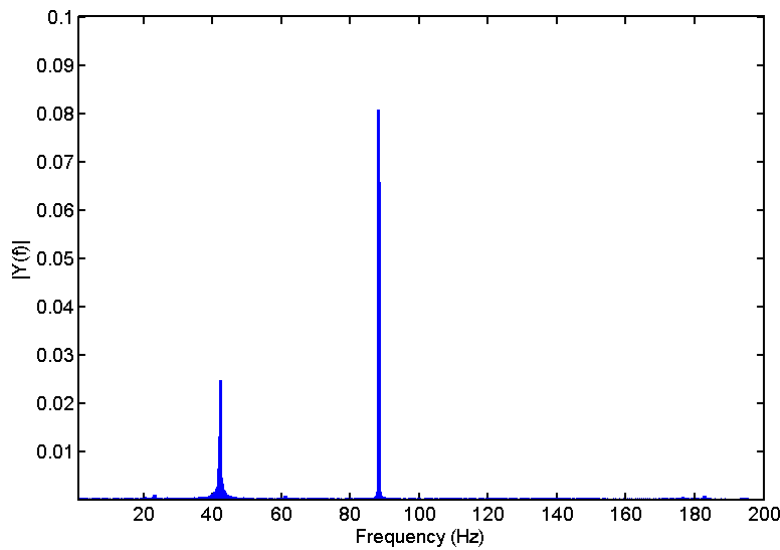


FIGURE 12 - FREQUENCY SPECTRUM OF THE OPTO-SENSOR SIGNALS

In figure 12 it can be seen that there is a huge peak at the actuation frequency of 88Hz. Also, some signal content is seen at 42Hz. This is the first swing mode, which is excited by the disturbances. Some smaller disturbances are seen at 23Hz, the shaker's eigenfrequency, 61Hz, the second Eigenmode of the tube, and 185Hz, the second swing mode. These disturbances have almost no influence on the measured flow and will therefore be ignored.

Recall from paragraph 2.2 that only the measured disturbances in y-direction are used. These have 50dB more contribution to the flow error than any other disturbance. The y-direction is seen from the CMFM coordinate frame. In figure 10 the coordinate frame is depicted.

In the next paragraph, the CMFM will be turned off, i.e. the twist mode is not actuated, in order to come up with a disturbance model from y-disturbances, a_y , to swing motion. In paragraph 3.3, this model will then be used to predict the disturbance influence. Here the CMFM is turned on to determine the effectiveness of the influence on the flow measurement by this prediction filter. The last paragraph of this chapter uses the same data to validate the workings of a band-pass filter.

3.2 GAIN ESTIMATION

The y-disturbances a_y and the swing motion are measured for 60 seconds. The transfer function, from applied disturbances to Coriolis displacement, is estimated using MATLAB's system identification toolbox, Ident. For this purpose actuation of the CMFM is turned off, such that only the motion caused by the floor vibrations is measured.

The measured data are translated to Cartesian coordinates and imported in Ident. After detrending the data, a second order state space model is estimated. There are two opto-sensors in the CMFM, so this is done twice ultimately giving two transfer functions. These estimated transfer functions are then compared to the derived transfer (2.26). This is shown in figure 13.

Before the estimated transfers are evaluated, recall from paragraph 2.1 that only disturbances around the actuation frequency are of interest. The actuation frequency lies at 88Hz or 553rad. At this frequency, the response in (2.27) simplifies to

$$\frac{V_{out}}{V_{in}} = \frac{g}{\omega_{act}^2} \quad (3.1)$$

meaning that the transfer is mostly affected by a changing actuation frequency and not by a change in the swing frequency, i.e. a change in the third instead of the first eigenmode (see paragraph 2.2).

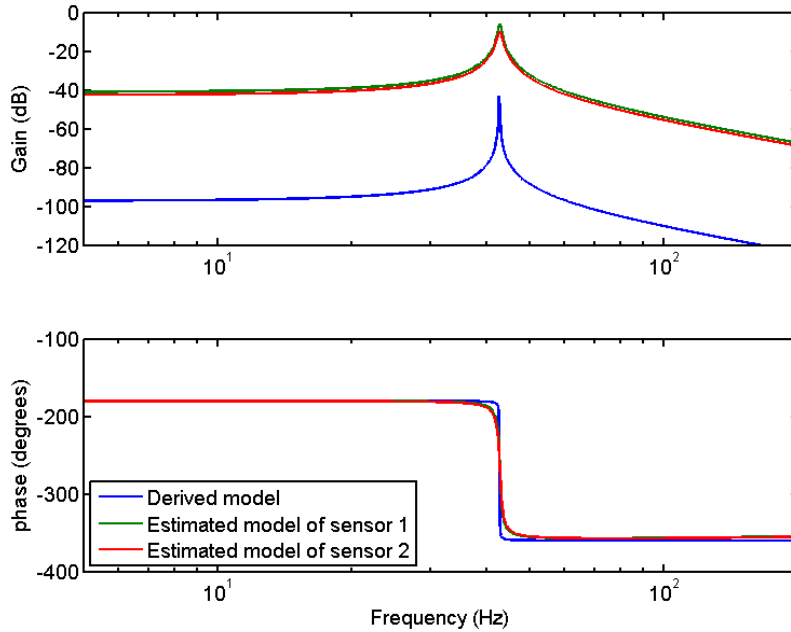


FIGURE 13 - ESTIMATED TRANSFERS FROM FLOOR ACCELERATIONS TO CORIOLIS DISPLACEMENT

It can be seen that there are two deviations between the estimated transfers and the model. Firstly, the system is modeled without any damping, but the real system has a little damping. This does not influence the transfer at the actuation frequency and is therefore not important. Secondly, the gain is not correct in the estimated model. The gain parameter of the derived transfer (2.26) was set to -1. The correct gain is calculated by dividing the derived gain by the estimated gain at the actuation frequency. For sensor 1 the gain is found to be -644 and for sensor 2 it is -539 . Using these gains a prediction filter is constructed.

3.3 PREDICTION FILTER

As stated in paragraph 2.4, disturbances at the actuation, and thus Coriolis frequency, are rejected by predicting the influence of external vibrations at this frequency. In this paragraph, the workings of this prediction filter are tested without the influence of a band-pass filter. A summary of the algorithm is depicted in figure 14. Due to practical restrictions, a notch filter is implemented, but only for calculating the residual used for the measurement update. This filter does not enhance the processed signal.

The filter is implemented with the gains from the previous paragraph and a process covariance based on an estimated model uncertainty of 1 percent. The measurement correlation value is 0.001, which is equal to the actual noise level. From these uncertainties, the measurement matrix (2.32) and the state transition matrix (2.29), the steady Kalman gain matrix is calculated and found to be

$$K_1 = [0.0021 \quad 0.0031]^T \quad (3.2)$$

Despite the high sampling rate, the found values for K_1 are rather low. This indicates that the filter relies on the model and assumes that information to be correct. This also means that measurement corrections are small.

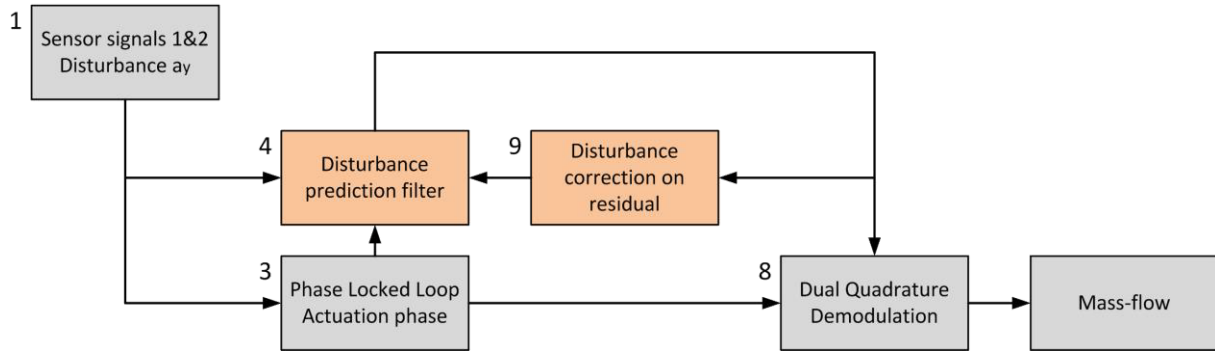


FIGURE 14 - FLOW CALCULATION WITH PREDICTION FILTERING

The disturbances measured by the acceleration sensor are fed to the prediction filter. The sensor gains found in paragraph 3.2 of -644 and -539 for sensor 1 and 2 respectively are used in the input matrix of (2.29). The flow is calculated using the DQDM scheme from section 2.1.

The result of the Kalman filtering is seen in figure 15. This filter gives 17.3dB disturbance attenuation on the measured flow. This is calculated by comparing the standard deviations of both the filtered and the unfiltered flow. It took 27 seconds to execute this filtering on 60 seconds of data.

Decreasing the uncertainty of the model increases the attenuation. By changing the model uncertainty to 0.1 percent a steady Kalman gain matrix becomes

$$K_2 = [0.00076 \quad 0.0011]^T \quad (3.3)$$

Implementing the filter with this gain matrix results in 18.1dB disturbance attenuation. The cause for this is not found in the operation of the Kalman filter but in the disturbance measurement.

Although notch filtering removes almost the entire actuation signal, some is still left in the measurements. When information at the actuation frequency is fed to the Kalman filter it is seen as an external disturbance and therefore the filter removes a signal that originally wasn't there.

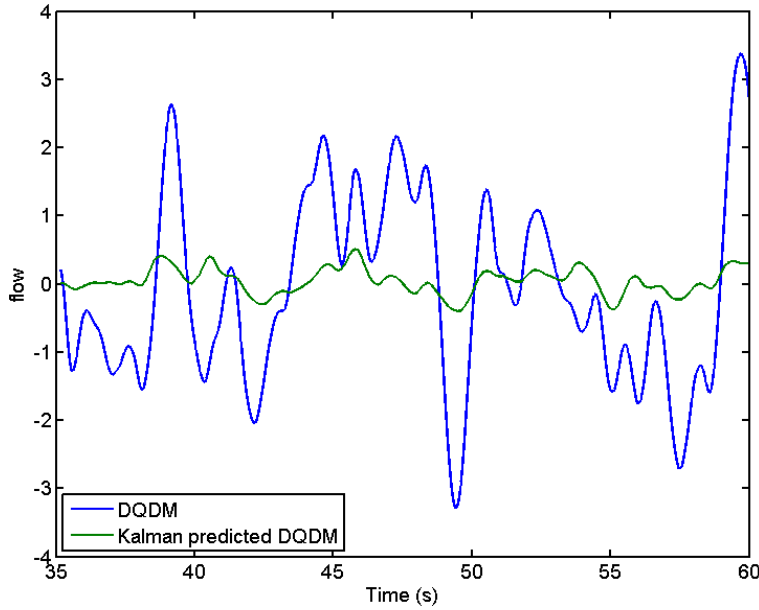


FIGURE 15 - FLOW BEFORE AND AFTER REMOVING THE KALMAN PREDICTED DISTURBANCE

Furthermore, disturbances at other frequencies than the actuation frequency are not important for the Kalman filter since they are later removed by either the notch filter or the low-pass filter in the DQDM. With this in mind, the correction is disabled, i.e. the Kalman gain is set to zero, such that no measurement updates occur. To prevent the estimated signal from growing unbounded, a little damping is added to the state transition matrix. The damping factor is based on the high Q-factor of the system. However, due to sensor noise the damping value cannot be too small as this noise continuously adds energy to the filter. The damping can be seen as the factor smaller than 1 by which the velocity is multiplied to obtain the new velocity. The new state transition matrix now becomes

$$F = \begin{bmatrix} 1 & T_s \\ \omega_{swing}(n)^2 \cdot T_s & 0.999 \end{bmatrix} \quad (3.4)$$

Disabling the update improves the disturbance attenuation to 19.2dB and reduces processing time to 22 seconds.

Next, the gains found in paragraph 3.2 are altered to check whether they are optimal. Some tuning finally gives a 20.7dB attenuation for gains of -686 and -582 for sensor 1 and 2 respectively.

To gain some more insight in the effect of a mismatched gain, some experiments are done in which this gain is varied. The result on the filter's attenuation is plotted versus a gain error percentage and depicted in figure 16. This is done for multiple disturbance levels.

From figure 16 it can be seen that a gain match within 3% of the actual gain is sufficient for estimating the disturbance influence. When the gain is known accurately, there are other causes why the attenuation no longer increases. These causes can be found in the noise levels of the sensors. For this test, the calculation of the y-acceleration is based on multiple sensors causing errors to add up.

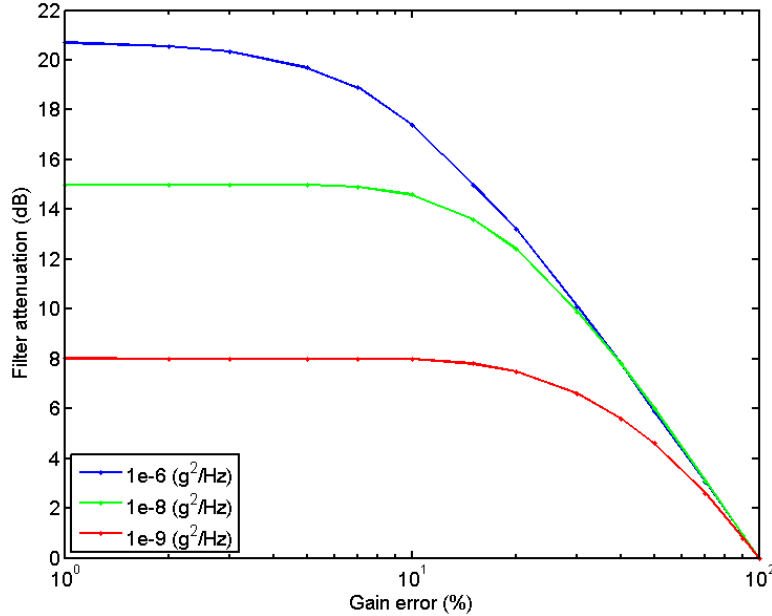


FIGURE 16 - GAIN ERROR VERSUS FILTER ATTENUATION

When the disturbance level decreases, the filter has less attenuation. If no intentional external disturbances are presented to the CMFM, the prediction filter still improves the measurement value by 0.2dB. The measured disturbance level with no intentional external vibrations has an order of magnitude of $1e^{-11} (g^2/Hz)$. It is also noted that the prediction filter adds no delay whatsoever to the response.

It is noted that the exact gains are not so relevant as long as the total gain is equal to -1268. The reason for this can be found in the Dual Quadrature Demodulation. Here, the phases of the signals are summed when determining the flow. The predictor subtracts the extra phase caused by a disturbance. In the end, it is not important on which of the two sensor signals this correction is applied as long as the total correction is right. This is for a total gain of -1268.

An attempt is made to estimate the gain using online measurements. This requires extra filtering using comb filters as is expounded in Appendix B: Online Gain Estimation and DQDM Filtering.

In the next paragraph, a band-pass filter is added to the algorithm. First, the filter will be discussed after which the result of both prediction and notch filtering are evaluated.

3.4 NOTCH FILTER

A notch filter is implemented for filtering disturbances around the actuation frequency. The prediction filter is disabled. The processing algorithm with only a notch filter is summarized in figure 17.

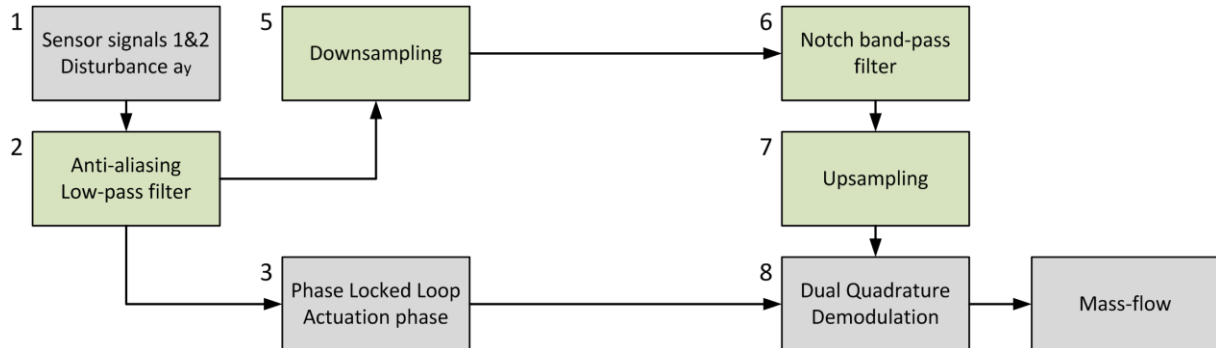


FIGURE 17 - FLOW CALCULATION WITH NOTCH FILTER

The implemented filter has a bandwidth of 0.34Hz. This is the theoretically required bandwidth from (2.37) with 0.1Hz extra uncertainty from the actuation frequency estimation. The 0.34Hz bandwidth corresponds to $\rho = 0.999533$. The notch-filtered result is compared to a flow calculation without notch filter called the measurement. The result can be seen in figure 18.

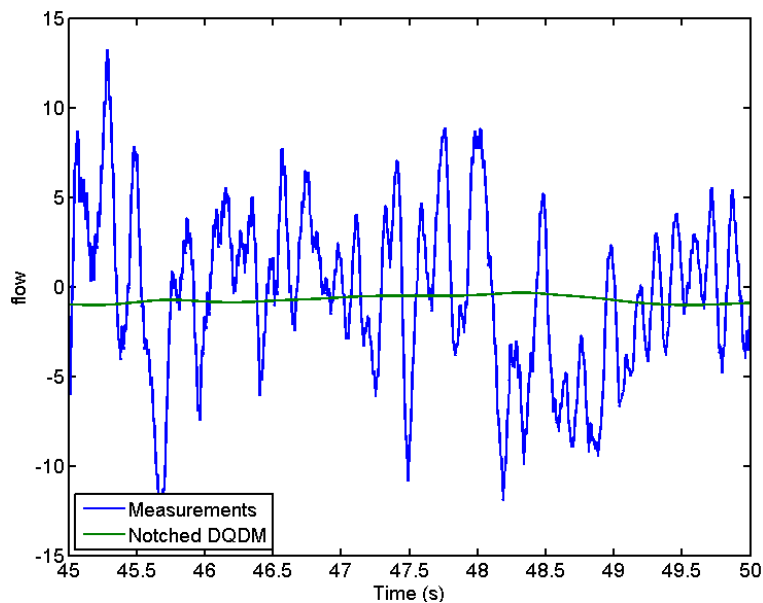


FIGURE 18 - THE NOTCH FILTERED FLOW COMPARED TO THE MEASUREMENTS

The notch filter attenuates the disturbances by 24.5dB. This value is calculated by comparing the standard deviation of both signals.

As the notch filter is a resonance filter with memory, it is interesting to check the response time. The filter's response to a step change in the flow is simulated. The result of this simulation for a 0.34Hz bandwidth can be seen in figure 19.

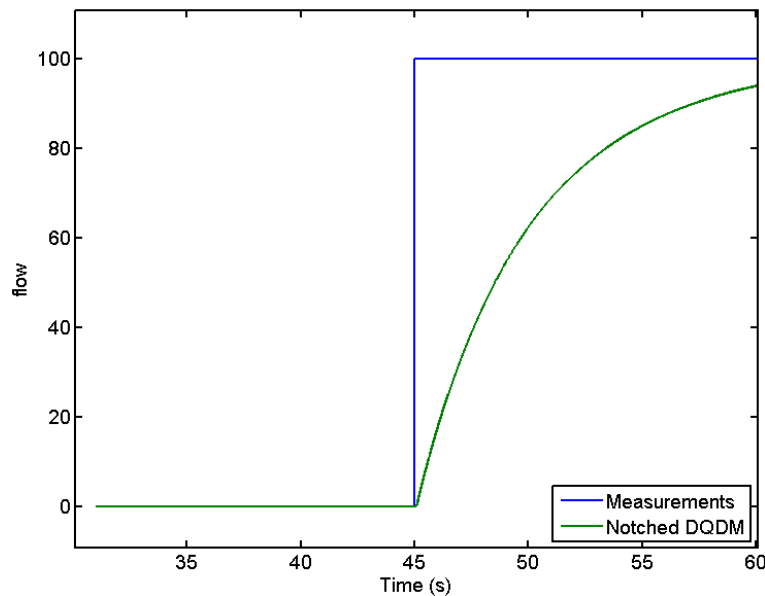


FIGURE 19 - RESPONSE OF THE NOTCH FILTER TO A STEP RESPONSE IN THE FLOW AT T=45S

The step in figure 19 shows that the response time of the filter is in the order of 20 seconds. This is the time at which the filter reaches its final value plus or minus 1 percent.

To further evaluate the notch filter, its bandwidth is compared to the response time and depicted in figure 20.

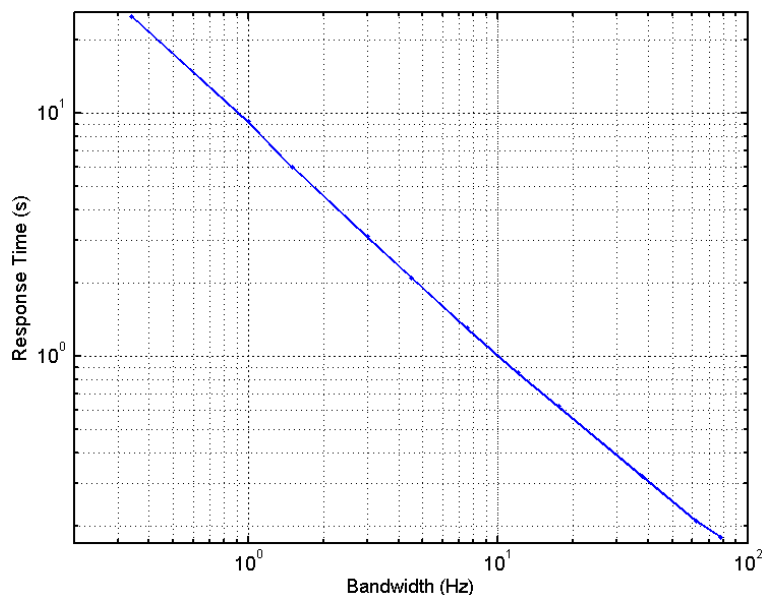


FIGURE 20 - NOTCH FILTER BANDWIDTH VERSUS RESPONSE TIME

From figure 20 it is concluded that a 1 second response time corresponds to a notch bandwidth of 10Hz.

The relation between filter bandwidth and attenuation is also interesting. This is depicted in figure 21.

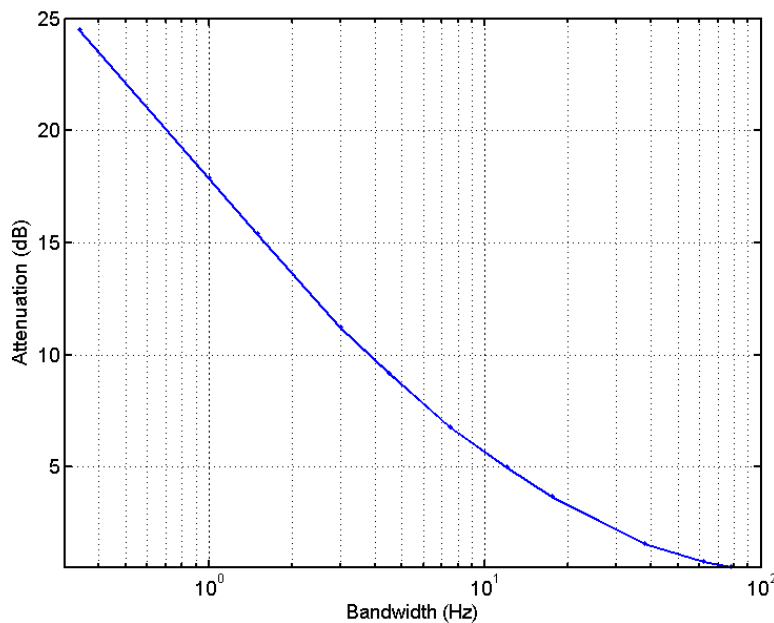


FIGURE 21 - NOTCH FILTER BANDWIDTH VERSUS ATTENUATION

From this figure, it can be seen that the aforementioned 10Hz filter bandwidth corresponds to 6dB attenuation.

A variable can be added to the notch filter which checks whether the filter still correctly filters the signal (9). This variable can simply check if the output of the filter has more signal content than the removed disturbances. If it does, the bandwidth can be reduced towards its theoretical minimum of 0.34Hz. If this variable indicates that the filtered signal is not correct, the bandwidth is immediately set to 10Hz in order to obtain the required response. This ensures that the filtered signal contains the flow information while achieving maximum attenuation.

In general, it can be stated that higher order filters introduce a larger delay. Also, the smaller the pass-band, the larger the delay becomes. There is always a trade-off between delay and noise attenuation. The adaptive notch filter, that can vary both the notch frequency and the filtered bandwidth, is a good solution to this problem. This enables maximum noise attenuation for a stable flow and a fast response for varying flow signals.

The filter's robustness against varying actuation frequencies is checked and it is found to track changes up to 4Hz per second.

After removing as much disturbances as possible, a prediction filter is now added to estimate the disturbances at the unfiltered frequency and further improve the measurements.

When adding a prediction filter to the notch filter, the total result of the algorithms is found. Here, a notch filter width of 10Hz is used. The flow result after applying prediction and notch filtering is seen in figure 22.

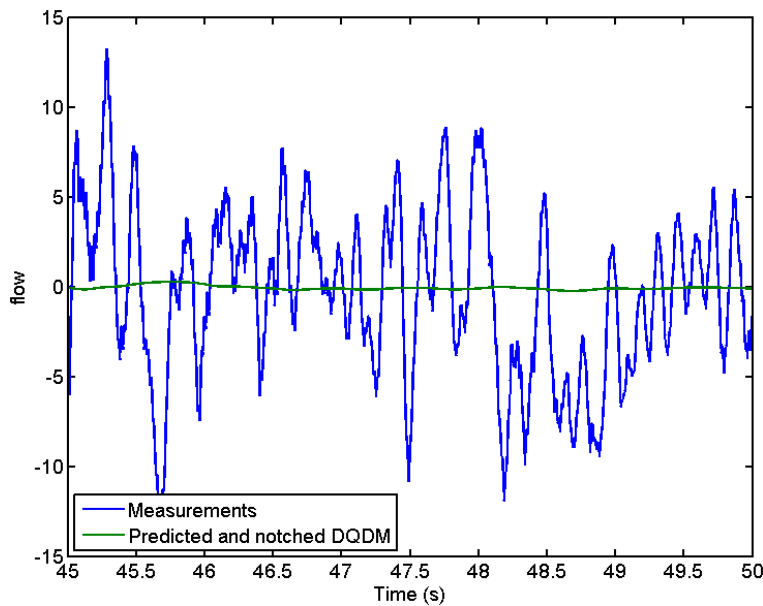


FIGURE 22 - PREDICTION AND NOTCH FILTERED FLOW COMPARED TO THE UNFILTERED FLOW

After applying both algorithms, a total attenuation of 22.1dB is obtained and it took 28 seconds to process 60 seconds of data. This is without the notch filter converging its bandwidth. For steady flows, the notch bandwidth decreases towards 0.34Hz and the total attenuation becomes 40.3dB. Here, the total attenuation is not the sum of the individual attenuation of the filters. This means that the prediction filter removes disturbances that cannot be attenuated by the notch filter.

4 CONCLUSION

From this research on the attenuation of external vibrations using filtering techniques, two conclusions are drawn. The results are summarized in table 1.

Firstly, with the prediction of the influence of external vibrations by a Kalman filter, an attenuation of 20.7dB is achieved. For this filter to operate properly, the gain at the actuation frequency has to be known. This was determined by estimating the transfer function from floor vibrations to the measurement error. The measurement update of the filter should be disabled if the measurements for correction have signal content at the actuation frequency. This causes the filter to base its estimation on non-existing disturbances, which worsens the filter output and can eventually even worsen the measured mass-flow.

TABLE 1 - OVERVIEW OF THE DISTURBANCE ATTENUATION PER FILTER

	Response time	-	Kalman $1e^{-6} (g^2/Hz)$	Kalman $1e^{-8} (g^2/Hz)$	Kalman $1e^{-9} (g^2/Hz)$	Kalman $1e^{-11} (g^2/Hz)$
-	0.1s	0dB	-20.7dB	-15dB	-8.1dB	-0.2dB
Notch 10Hz	1s	-6dB	-22.1dB			
Notch 0.34Hz	20s	-24.5dB	-40.3dB			

Secondly, time domain filtering can massively improve the signal to noise ratio of the measured signal. The required bandwidth for filtering the sensor signals is theoretically 80 times smaller than for filtering the calculated phase. Therefore, in theory 38dB attenuation can be achieved. A notch filter of 0.34Hz showed 24.5dB improvement in practice, but as it is a resonance filter the response time was over 20 seconds. This can be solved by letting the filter converge towards a small bandwidth and check if the filtered signal has no actuation signal content. This is done by increasing the ρ -parameter. If the signal is lost, the notch bandwidth is set to 10Hz. This attenuates the noise by 6dB while obtaining a desired response time of 1s.

A practical attenuation of 22.1dB is achieved with a combination of the prediction and notch filter. If the notch filter fully converges its bandwidth to its theoretical minimum of 0.34Hz, i.e. for steady flows, this attenuation increases to 40.3dB for high disturbance levels.

5 DISCUSSION

This research showed that it is possible to obtain a reasonable attenuation of external disturbance using a prediction filter. The notch filter however, caused an undesired large response time. Therefore, it is interesting to look further into filtering the sensor signals in the time domain. For instance, adaptive FIR filtering with a small pass-band around the actuation frequency can be an option. Although this costs a lot of computational power, band-pass filtering creates a theoretical improvement of the SNR of 38dB.

Furthermore, it is known that the tube window's rotation pole (the point on the bottom tube around which the window twists) shifts from the expected twist axis. With the sensor gains known, the rotation pole of the tube window can be calculated based on the measured signal amplitudes. The PLL is able to estimate these amplitudes and, as the positions of the sensors are known, the rotation pole has a simple linear relation with the measured signal amplitude.

Also, if the location of the rotation pole is known, this can be used to improve the disturbance estimate. The disturbance sensor is in the center of the CMFM. If the rotation pole is not exact in the center, this causes some of the actuation signal to be measured by the disturbance sensor. This has no real influence on the flow measurement and therefore it should not be in this estimated disturbance. It can be removed by measuring the actuation amplitude, the position of the rotation pole and the mass of the tube compared to the case. This gives a transfer from actuator motion to disturbance sensor by which the influence of actuator motion can be eliminated.

Another remark has to be made on the attenuation of crosstalk. If two CMFMs are placed close together the actuation signal of the one CMFM acts as an external vibration on the other CMFM and vice versa. As the actuation frequencies of similar devices are almost equal, this disturbance cannot be removed by regular filtering. The prediction filter presents a very good solution in this case as the crosstalk disturbance is measured by the acceleration sensor and can thus be attenuated.

Furthermore, the prediction filter works better if more disturbance is present. That way the noise level of the acceleration sensors play a less crucial role and thus more attenuation can be achieved. It should be noted that for this to be true, the gains have to be determined accurately. However, the filter still attenuates disturbances if no intentional external disturbances are presented to the CMFM.

Instead of adding extra band-pass filters, also an attempt could be made to construct a varying low-pass filter in the DQDM scheme. This filter can also converge for steady flows and react to a flow change by increasing the bandwidth.

The last remark is made on the actuation frequency. A higher actuation frequency allows for easier filtering. Due to the mixing, the low-pass Bessel filter can more easily remove the disturbance frequencies if they are further away from the actuation frequency in an absolute sense. This doesn't hold for the notch filter. With an increased actuation frequency the total delay due to filtering is decreased as phase delays at higher frequencies cause smaller time delays. The required low-pass filters can be of lower order, without loss of performance.

REFERENCES

1. **Anklin, M.** Coriolis mass flowmeters: Overview of the current state of the art and latest research. *Flow Measurement and Instrumentation*. 2006, Vol. 17, 6, pp. 317-323.
2. **Ridder, L. van de.** Active vibration isolation feedback control for Coriolis Mass-Flow Meters. *Control Engineering Practice*. 2014, Vol. 33, pp. 76-83.
3. —. Quantification of the influence of external vibrations on the measurement error of a Coriolis mass-flow meter. *Flow Measurement and Instrumentation*. August 29, 2014, pp. 39-49.
4. **Mehendale, A.** *Coriolis Mass Flow Meters For Low Flows*. Enschede : Print Partners Ipskamp, Enschede, 2008.
5. **Aarts, R. and J. Meijaard, J. Jonker.** SPACAR 2013 - Manual. *University of Twente*. [Online] March 14, 2011. [Cited: 10 14, 2014.]
<http://www.utwente.nl/ctw/wa/software/spacar/2013/manual/>.
6. **Heijden, F. van der.** *Classification Parameter Estimation & State Estimation An Engineering Approach Using MATLAB*. West Sussex PO19 8SQ, England : Wiley, 2004.
7. **Yuan, J.** Adaptive Laguerre filters for active noise control. *Applied Acoustics*. 2007, Vol. 68, pp. 86-96.
8. **Ciochină, S.** *Adaptive Notch IIR Filters an implementation on Motorola SC140*. Bucharest, Romania : University of Bucharest, Faculty of Electronics and Telecommunications, 2003.
9. **Shen, T.** A Novel Time Varying Signal Processing Method for Coriolis Mass Flowmeter. *Review of Scientific Instruments*. 065116, 2014, Vol. 85.
10. **Wu, B.** A Magnitude/Phase-Locked Loop Approach to Parameter Estimation of Periodic Signals. *IEEE Transactions On Automatic Control*. 2003, Vol. 48, 4, pp. 612-618.
11. **Tjepkema, D.** *Active hardmount vibration isolation for precision equipment*. Enschede : University of Twente, 2012.

APPENDIX A: PHASE LOCKED LOOP

In this research, some Phased Locked Loops, PLLs, were used for estimating phases and frequencies. Here, the workings of such a PLL are explained.

In general, a PLL is used to estimate or track the parameters of a slowly varying periodic signal. In this case, the actuation signal is tracked by a PLL. This is done for 3 reasons. Firstly, the force actuator for the twist mode requires the phase of the actuator motion in order to actuate correctly. The reason for this is found in the fact that the tube is actuated in resonance such that a large actuation amplitude can be obtained with little actuation energy. Secondly, the signal processing uses the actuator phase for mixing and predicting. Furthermore, the notch filter requires the signal frequency to assure setting the correct notch frequency. All of this information is gathered by a PLL.

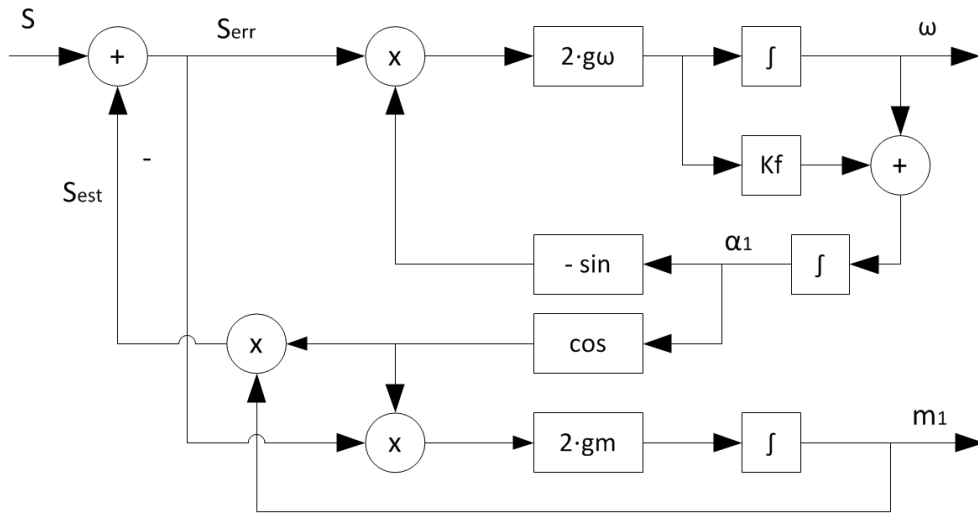


FIGURE 23 - PHASE LOCKED LOOP

The PLL extracts the frequency (ω), phase (α_1) and amplitude (m_1) (10) from a periodical signal. The scheme in figure 23 is used to derive the PLL update equations. Note that the system is discretized which requires an estimated $\hat{\alpha}_1(n)$ for causality.

$$\hat{\alpha}_1(n) = \alpha_1(n-1) + \omega(n-1) \cdot T_s \quad (0.1)$$

$$S_{est}(n) = m_1(n-1) \cdot \cos(\alpha_1(n)) \quad (0.2)$$

$$S_{err}(n) = S(n) - S_{est}(n) \quad (0.3)$$

$$\omega(n) = \omega(n-1) - \sin(\alpha_1(n)) \cdot 2 \cdot g_\omega \cdot S_{err}(n) \cdot T_s \quad (0.4)$$

$$\alpha_1(n) = \hat{\alpha}_1(n) + K_f \cdot (\omega(n) - \omega(n-1)) \quad (0.5)$$

$$m_1(n) = m_1(n-1) + \cos(\alpha_1(n)) \cdot 2 \cdot g_m \cdot S_{err} \cdot T_s \quad (0.6)$$

where the design parameters g_m , g_ω and K_f determine the trade-off between convergence time and disturbance rejection for respectively the amplitude, frequency and phase. T_s is the sample time.

The parameter g_m should be as low as possible, as it is a direct feed through for disturbances. The other parameters are also tuned to be as low as possible, but have to be able to track a 4Hz frequency change per second, at the typical resonance frequency of 88Hz, and a step change in the flow. The parameters are found to be

$$K_f = 0.4 \quad (0.7)$$

$$g_\omega = 0.2 \quad (0.8)$$

$$g_m = 0.0001 \quad (0.9)$$

The PLL is capable of tracking the actuation frequency, ω , within 0.05Hz, even when disturbances are presented to the CMFM. This is depicted in figure 24.

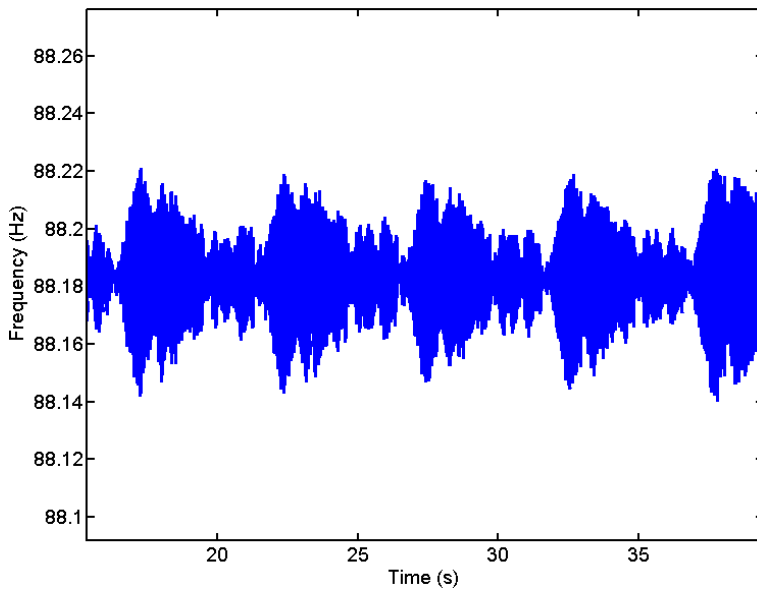


FIGURE 24 - ESTIMATED ACTUATION FREQUENCY WITH EXTERNAL DISTURBANCE

Not only is the actuation frequency present in the signal, also some higher harmonics are detected. In an attempt to improve the stability of the PLL, extra loops are added that estimate the second and third harmonic of the actuation signal.

A signal flow diagram of the improved PLL can be seen in figure 25.

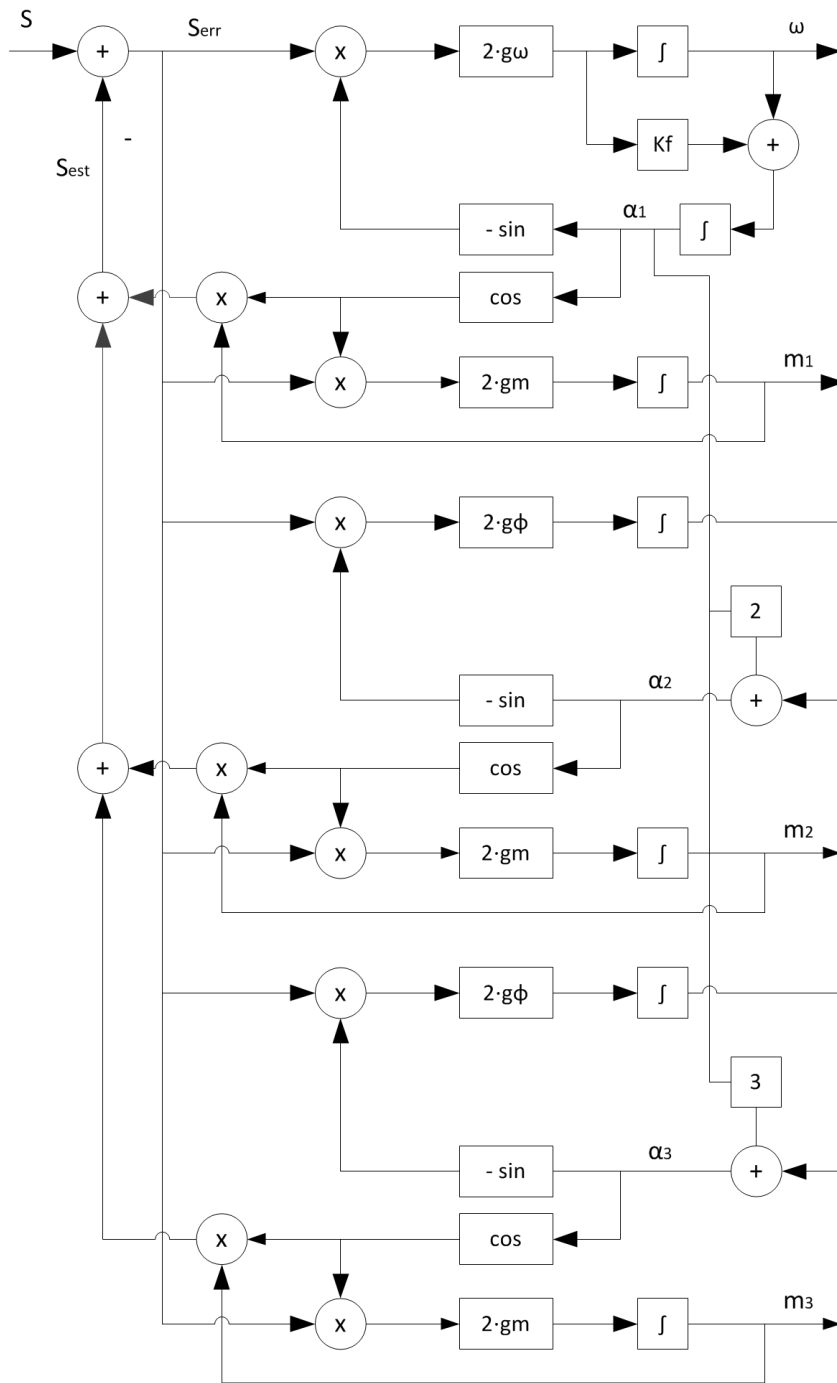


FIGURE 25 - IMPROVED PHASE LOCKED LOOP

Update equations for the second and third harmonic are added to the PLL-algorithm. The result for the actuation frequency is depicted in figure 26.

The estimation of the actuation frequency by the improved PLL is not visibly better. It is very likely that other disturbances have more influence on the frequency estimation. Looking at the average frequency compensates these disturbances. Most of the disturbances have an opposite influence than the actuation on the measurement; it causes a frequency shift in opposite directions. This is due to the actuation having π rad phase shift between the two sensors and the disturbances have no phase difference i.e. disturbances are a swing motion while the actuation is a twist motion. The average frequency gives a major improvement on the variance of the estimated frequency.

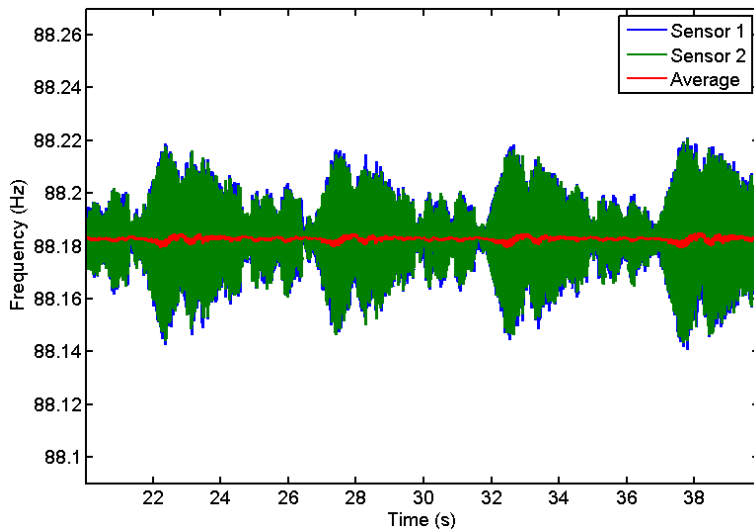


FIGURE 26 - IMPROVED ESTIMATION OF THE ACTUATION FREQUENCY

Next, an attempt is made to remove the disturbance frequency of 42Hz by means of a PLL. Although this PLL is able to correctly estimate the frequency, it is unable to follow the disturbance signal. This is because this signal is not periodic. It changes frequency, phase and magnitude a lot. The PLL is able to predict the average disturbance, and thus the frequency, but cannot remove this signal.

Since the PLL is able to calculate the phase of each measured signal, it can also be used for flow calculation. Recall that the flow is direct measure of the phase difference between the two sensor signals. With this in mind, two PLLs are implemented after filtering and the flow is calculated by multiplying the phase difference with the sensor sensitivity.

Both the standard deviation and the response time are measured for this flow measurement and compared to the DQDM flow calculation. From experimental results it is concluded that a PLL gives 0.5dB less attenuation than the DQDM. Also, it has a 0.5s slower response for flow changes. This is due to the fact that the PLL acts as an extra filter around the actuation frequency estimate. Since this information is already filtered, the PLL does not improve the measurement. The parameters K_f and g_ω can be tuned to improve the response time, but this would worsen the attenuation. With this information it is concluded that DQDM is the better option for flow calculation.

APPENDIX B: ONLINE GAIN ESTIMATION AND DQDM FILTERING

For easy implementation of the prediction filter, it is helpful to estimate the gains from the disturbance sensor to the measurements online. This enables the filter to be implemented without any calibration procedures. The easiest way of online estimation is by means of a Recursive Least Squares algorithm. The RLS algorithm requires a regressor. This regressor is a variable that is altered in such a way that the square of a certain error is minimized. In this case it seems obvious to look at the system as two single input single output systems and use the gain for each system as regressor. The error should then be defined on the output of the measurement algorithm. However, there is a problem with this definition. Since the flow is unknown the error cannot simply be defined as the output. If that were done, the regressor will also try to minimize the flow output, which can result in an incorrect flow measurement. Furthermore, the disturbance causes only a small fluctuation of the flow around the measurement value. It is impossible to measure the small influence of a gain variation compared to all variables influencing the measurement output.

In an attempt to enable online gain estimation the signal is filtered. In this case a comb filter is implemented to attenuate two disturbances. The comb filter is a relatively simple FIR filter that removes a signal with a certain frequency by subtraction or addition. There are two types of comb filters. The first comb filter subtracts the sample from 1 comb frequency period ago from the current sample successfully removing the double comb frequency, its even harmonics and the DC value. The second filter adds the sample from 0.5 period ago to the current sample and therefore removes the comb frequency and the uneven harmonics. To get 0dB gain at the actuation frequency the calculated value is divided by 2. The frequency response of the filters is seen in figure 27.

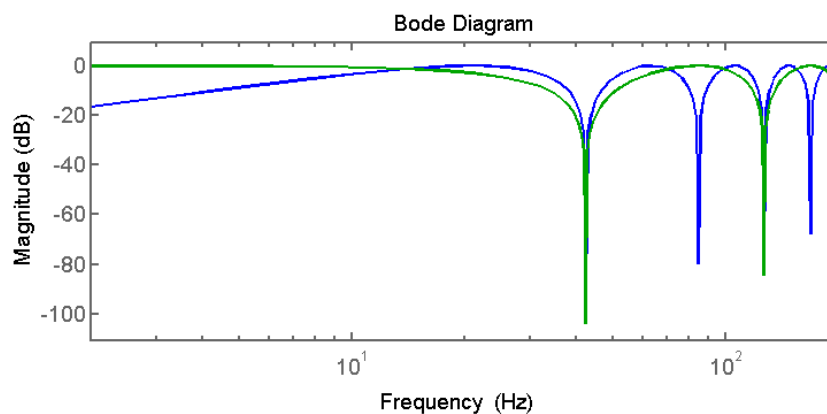


FIGURE 27 - COMB FILTER RESPONSE WITH ADDITION (BLUE) AND SUBTRACTION (GREEN)

Using the fact that the actuation frequency is close to the second harmonic of the disturbance, a comb filter with addition should be used as it removes the uneven harmonics. As the sample frequency is not always an exact multiple of the filtered frequency an interpolation between two samples is used in order to obtain the correct addition value.

The comb filter is added in two places during the DQDM scheme to enhance the signal. This should enable gain estimation. In figure 28 the total DQDM is depicted.

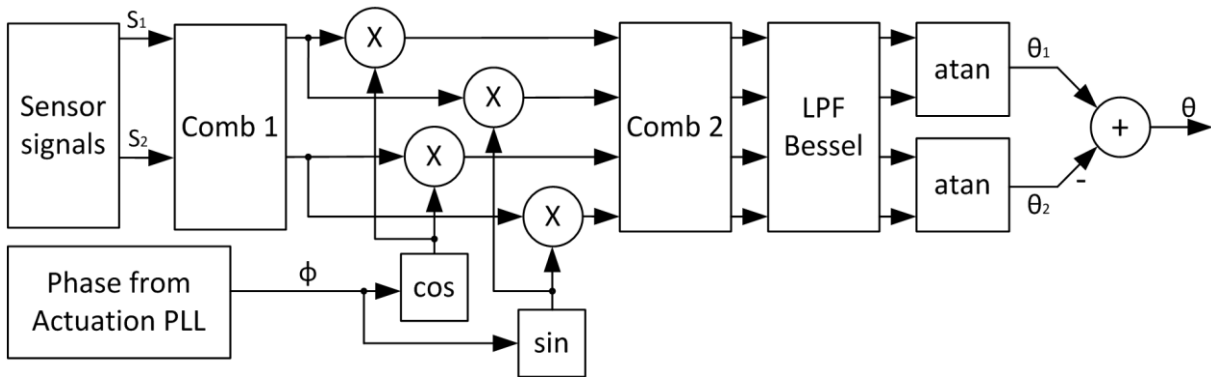


FIGURE 28 - DQDM SCHEME WITH COMB FILTERS

Compared to the original DQDM scheme of paragraph 2.1, the one depicted in figure 28 has two extra blocks. In the beginning, the swing mode of 42Hz is removed by means of a comb-filter. Here, it is kept in mind that the second harmonic is close to the actuation frequency. Therefore, an additive comb filter, which suppresses the uneven harmonics, is used such that no information is lost. This works very well and massively enhances the signal for further processing. Then, after mixing, the second harmonic of the mixing frequency is also attenuated using a comb filter. This time it should be kept in mind that the information of the actuation signal has shifted towards DC. Again an additive comb filter is used to preserve information around DC and remove the second harmonic generated by mixing the signal. The responses of the comb filters are depicted in figure 29.

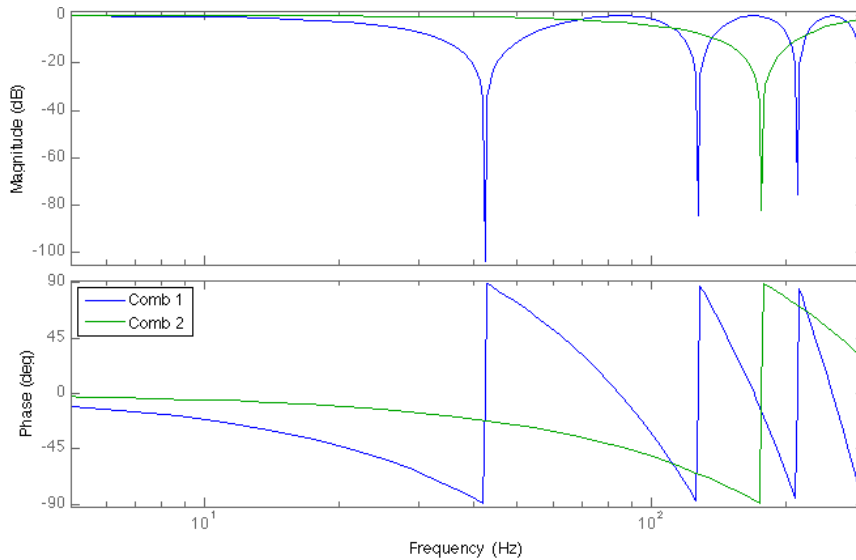


FIGURE 29 - BODE PLOT OF THE COMB FILTERS

Next, low-pass filters are added that remove more of the noise, finally obtaining a stable angle measurement. After filtering, the online gain estimation is implemented using a grid search.

To enable gain estimation, the outcome of the filtering algorithm is also calculated for two extra gain values. One is twice the estimated gain and the other is zero. Recall from paragraph 3.3 that a 100% error in the gain estimation gives the same result as no prediction filtering. If the real gain estimate is correct, both the bigger and the smaller gain should produce the same error. When one of them produces a larger error, this one is less correct and the gain estimate should move in opposite direction. For instance, when the signal filtered with the double gain gives a larger error than the signal with no prediction filter, the estimated gain is too big. Only if both calculated errors are equal, the estimated gain is correct. The error has to be calculated for low-frequency changes, as it represents the measurements at the actuation frequency. With this in mind, each new sample is compared to a moving average of the signal. The moving average is roughly the same for both the smaller and the bigger gain.

Implementation of this algorithm does not give the desired result, as the estimated gain is not stable. The cause for this is that the differences that need to be measured are smaller than the noise present in the system. These differences are seen if a large amount of samples with a constant flow is taken at once, such that all samples can add to the estimation. If a working algorithm can be found it might also be useful to enable the estimation only if the measured disturbance is above a certain threshold.